Molecular Mechanism of Onset and Progression of Nonalcoholic Steatohepatitis (NASH)

January 2014

Nobuya KURIKAWA

Molecular Mechanism of Onset and Progression of Nonalcoholic Steatohepatitis (NASH)

A Dissertation Submitted to
the Graduate School of Life and Environmental Sciences,
the University of Tsukuba
in Partial Fulfillment of the Requirements
for the Degree of Doctor of Philosophy
(Doctoral Program in Biological Sciences)

Nobuya KURIKAWA

Table of Contents

	Page
Abstract	**1**
Abbreviations	**4**
General Introduction	**6**
Chapter I	
“Effects of stearoyl-CoA desaturase-1 on the onset of NASH”	**10**
Introduction	**11**
Materials and Methods	**14**
Results	**20**
Discussion	**24**
Chapter II	
“Effects of angiotensin II on the progression of liver fibrosis”	**29**

Introduction **30**

Materials and Methods **32**

Results **39**

Discussion **44**

General discussion **48**

Acknowledgements **51**

References **53**

Tables **70**

Figures **75**

Abstract

Nonalcoholic steatohepatitis (NASH) is defined as abnormal lipid accumulation in the liver and subsequent liver injury, inflammation and fibrosis, which is concerned with obesity, insulin resistance and other metabolic disorders and sometimes progresses to liver cirrhosis and hepatocellular carcinoma. However, the molecular mechanism of the onset and progression of NASH is poorly understood. In order to elucidate the molecular mechanism, I focused on two crucial processes in NASH pathology, the onset process and the progression of liver fibrosis.

Stearoyl-CoA desaturase-1 (SCD-1) catalyzes the biosynthesis of monounsaturated fatty acids from saturated fatty acids and regulates triglyceride synthesis. The abnormality of SCD-1 seems to be responsible for obesity, insulin resistance, and hepatic steatosis. In order to elucidate the effects of SCD-1 on the onset of NASH, an SCD-1 inhibitor was administered to rats fed with methionine and choline-deficient (MCD) diets for 8 weeks, which showed hepatic steatosis, liver injury, inflammation and early fibrosis. Administration of the SCD-1 inhibitor decreased triglyceride accumulation in the liver of MCD rats. Administration of the SCD-1 inhibitor also attenuated the increase of plasma AST and ALT. Hepatic steatosis, hepatocellular degeneration, inflammatory cell infiltration and early fibrosis were histologically observed in liver of MCD rats, and administration of the SCD-1 inhibitor ameliorated these crucial problems in NASH. These results suggest that the SCD-1 inhibitor prevented hepatic steatosis and decreased sensitivity to the onset of the NASH phenotype including liver injury, inflammation and fibrosis.

Angiotensin II (Ang II), a major component of renin-angiotensin systems, possibly plays an important role in the pathogenesis of liver fibrosis which is the most crucial phenotype in chronic liver disease including NASH. In order to elucidate the effects of Ang II on the progression of liver fibrosis, an Ang II type 1 receptor blocker (ARB) was administered to rats that received bile duct ligation (BDL), which are liver fibrosis models without hepatic steatosis. ARB treatment inhibited the accumulation of liver collagen. Activated hepatic stellate cells (HSCs), key players in liver fibrogenesis, were highly accumulated in the area of collagen deposition in the livers of BDL rats. Furthermore, these cells expressed

AT1 receptors. ARB treatment decreased the accumulation of □SMA expressing AT1 receptors as well as collagen deposition. The effects of Ang II on fibrogenic phenotypes in *in vitro* activated HSCs were also evaluated. Ang II stimulated proliferation and collagen synthesis in activated HSCs and ARB treatment completely blocked them. Additionally, pro-fibrogenic cytokines, transforming growth factor-β1 and connective tissue growth factor were up-regulated by Ang II stimulation through AT1 receptors, suggesting their involvement to Ang II-stimulated activation of HSCs. These results suggest that Ang II stimulates the key phenotypes of activated HSCs through activation of AT1 receptors and consequently leads to the development of liver fibrosis

In conclusion, I demonstrated that SCD-1 and Ang II plays key roles in the onset process and the progression of liver fibrosis in NASH, respectively.

Abbreviations

ACE: angiotensin-converting enzyme
α-SMA: α-smooth muscle actin
ALT: alanine aminotransferase
Ang II: angiotensin II
ARB: angiotensin receptor blocker
AST: aspartate aminotransferase
AT1: angiotensin II type 1
AT2: angiotensin II type 2
BDL: bile duct ligation
ChREBP: carbohydrate response element-binding protein
CMC: carboxymethyl cellulose
Col1a1-Luc Tg: rat collagen 1a1 promoter-luciferase transgenic
CTGF: connective tissue growth factor
DAB: 3,3'-diaminobenzidine tetrahydrochloride
DMEM: Dulbecco's modified Eagle medium
ECM: extracellular matrix
FCS: fetal calf serum
FFA: free fatty acid
GBSS: Gey's balanced salts solution
HBSS: Hanks' balanced salts solution
HSC: hepatic stellate cell
LXR: liver X receptor
MCD: methionine and choline-deficient
MCP-1: monocyte chemotactic protein-1
MUFA: monounsaturated fatty acid
NAFLD: nonalcoholic fatty liver disease
NASH: nonalcoholic steatohepatitis
Olmesartan: olmesartan medoxomil

PBS: phosphate-buffered saline
PDGF: platelet-derived growth factor
PG:Tween: polyethylene glycol: Tween 80
RAS: renin-angiotensin system
SCD: stearoyl-CoA desaturase
SD: Sprague-Dawley
SREBP-1c: sterol regulatory element-binding protein-1c
TBS: tris buffered-saline
TCA: trichloroacetic acid
TGF-β1: transforming growth factor-β1
TIMP: tissue inhibitor of metalloproteinase
VLDL: very low density lipoprotein

General Introduction

Nonalcoholic fatty liver disease (NAFLD), which is identified by excess lipid accumulation in the liver, is strongly associated with obesity, insulin resistance, type 2 diabetes, hypertension, dyslipidemia and metabolic syndrome (Farrell and Larter, 2006; Torres and Harrison, 2008). NAFLD is frequently observed in patients with metabolic disorders and about 10% of them progresses to nonalcoholic steatohepatitis (NASH), which shows histological observation of hepatocellular degeneration, inflammation and fibrosis in the liver in addition to steatosis. Some of NASH patients progress to liver cirrhosis and subsequently hepatocellular carcinomas, which are the end-stage of liver disease (Younossi et al., 2002). The population of NASH/NAFLD patients in advanced countries is increasing with the rise in obesity. Some clinical pilot studies have been performed with agents including insulin sensitizers, anti-dyslipidemic drugs, anti-obesity drugs and antioxidants (Marchesini et al., 2001; Harrison et al., 2003a, 2003b; Belfort et al., 2006; Gomez-Dominguez et al., 2006; Satapathy et al., 2006; Sanyal et al., 2010). Nevertheless, there is no established therapy for NASH/NAFLD at present (Malinowski et al., 2013).

The molecular mechanism of NASH/NAFLD remains poorly understood due to difficulties in elucidating the pathology. First, a liver biopsy is necessary to diagnose NASH and analyze the pathology in detail. Liver biopsy is highly invasive and has a high risk for complications such as bleeding and rare death. It is not realistic to repeatedly perform biopsies to observe the progression of the disease. Therefore, it is sometimes difficult to identify NASH patients particularly in early stages which are generally non-symptomatic. Although many researchers have tried to discover non-invasive biomarkers for NASH, there are no clinically validated biomarkers at present (Festi et al., 2013). Second, the background of metabolic disorders in NASH/NAFLD patients was very complicated. A lot of metabolic factors are dysregulated and the abnormal phenotypes are different among each patient. Therefore, it is hard to understand and find causative factors for NASH.

The “two hit theory” has been proposed for the mechanism of NASH onset and progression (**Figure 1**; page 76) (Day, 1998). The “first hit” is the lipid accumulation in the liver, which is caused by obesity, insulin resistance and other

metabolic disorders. Then, the “second hit” stimuli leads to liver injury, inflammation and finally fibrosis. Levels of fatty acids in liver are regulated by some processes including fatty acid uptake into liver, *de novo* fatty acid synthesis (lipogenesis), secretion from liver as very low density lipoprotein (VLDL) and fatty acid oxidation (**Figure 2**; page 77). In human obesity, the main mechanisms of lipid accumulation in liver are possibly due to increased fatty acid uptake and *de novo* lipogenesis caused by insulin resistance (Lewis et al., 2002). Plasma free fatty acids (FFAs) are mainly derived from adipose tissue and are released to plasma by the lipolysis of triglycerides in adipocytes. Insulin negatively regulates the lipolysis in adipocytes. Therefore, obesity-associated insulin resistance activates lipolysis and then plasma FFA levels are elevated. The expression of CD36 which regulates fatty acid uptake in the liver is also up-regulated in the liver of NAFLD patients (Greco et al., 2008). Increased plasma levels and liver uptake of FFAs lead to an excess influx and accumulation of FFAs in NAFLD liver. Furthermore, hyperglycemia and hyperinsulinemia resulting from insulin resistance can activate transcriptional factors regulating fatty acid synthesis in the liver including sterol regulatory element-binding protein (SREBP)-1c and carbohydrate response element-binding protein (ChREBP). In this manner, the increase of *de novo* lipogenesis may also cause lipid accumulation in NAFLD livers. Donnelly et al. has reported that 26% of liver triglyceride in NAFLD patients is derived from *de novo* lipogenesis compared with 5% in healthy persons (Donnelly et al., 2005). One important aspect of the two-hit theory is that steatosis *per se* is not causal in the development of NASH, but it sensitizes the liver to various second hit stimuli. Some factors such as oxidative stress, endotoxin and other bacterial components and inflammatory cytokines have been proposed as the second hits. However, the precise molecular mechanism is poorly understood.

Chronic injury and continuous inflammation in the liver lead to liver fibrosis and the progression of fibrosis finally causes cirrhosis and hepatocellular carcinoma, which are often lethal. Liver fibrosis is the predominant and most harmful process in NASH and is characterized by the abnormal accumulation of an extracellular matrix (ECM) such as collagen (Hernandez-Gea and Friedman, 2011). Fibrosis is generally observed in various chronic liver diseases including NASH.

Hepatic stellate cells (HSCs) are a major source of ECM in the liver, and HSCs account for approximately 5% to 8% of total cells in normal livers (Friedman, 2008). HSCs possess vitamin A droplets and produce small amounts of ECM components in normal conditions, which are called “quiescent HSCs.” In injured livers, HSCs morphologically transform to myofibroblast-like cells, characterized as having a proliferative, fibrogenic and contractile phenotype. Their transformed cells express α-smooth muscle actin (α-SMA), which are called “activated HSCs.” Activated HSCs can produce an excess of collagen and other ECM components and simultaneously inhibit ECM degradation by the induction of tissue inhibitor of metalloproteinases (TIMPs), resulting in ECM accumulation in the liver. In injured liver, some factors, which are produced from surrounding cells such as hepatocytes, Kupffer cells, sinusoidal endothelial cells and inflammatory cells, are thought to activate HSCs in a paracrine manner although the precise mechanism is poorly understood (Friedman, 2008). Transforming growth factor-β1 (TGF-β1) plays an important role in the activation of HSCs. TGF-β1 mainly stimulates the activation and collagen synthesis of HSCs in an autocrine or paracrine manner (Matsuoka and Tsukamoto, 1990; Gressner, 1995). It has been reported that a blockade of TGF-β1 by the injection of a soluble type or dominant-negative type of TGF-β1 type II receptors into animals, prevented experimental liver fibrosis (George et al., 1999; Qi et al., 1999; Yata et al., 2002). Thus, TGF-β1 is highly involved in the pathogenesis of liver fibrosis. Connective tissue growth factor (CTGF), a cysteine-rich protein that belongs to the family of CNN, is thought to act as a downstream mediator of the fibrogenic actions of TGF-β1, and also plays an important role in the development of fibrosis in a variety of organs (Leask et al., 2002). It was reported that CTGF mRNA was up-regulated in human liver cirrhosis or activated HSCs, and recombinant CTGF stimulated activation of HSCs (Paradis et al., 1999, 2002; Williams et al., 2000). In this manner, these two cytokines are thought to be highly concerned with activation of HSCs.

In my present study, in order to elucidate the molecular mechanism of NASH, I focused on two crucial processes, the onset of NASH and progression of fibrosis. I focused on stearoyl-CoA desaturase-1 (SCD-1) in the onset of NASH and angiotensin II (Ang II) in the progression of fibrosis as key factors.

Chapter I

“Effects of stearoyl-CoA desaturase-1 on the onset of NASH”

Introduction

SCD is an endoplasmic reticulum enzyme that catalyzes the biosynthesis of monounsaturated fatty acids (MUFAs) from saturated fatty acyl-CoAs (Ntambi, 1995). SCD, in conjunction with the NADPH, the flavoprotein cytochrome b5 reductase, and the electron acceptor cytochrome b5, introduces the cis double bond in the Δ9 position of fatty acyl-CoA substrates, preferentially stearoyl (C18:0) and palmitoyl (C16:0)-CoA. These MUFAs are used as substrates for the synthesis of triglycerides, cholesteryl esters, membrane phospholipids, and wax esters. Two human and four mouse SCD isoforms have been characterized (Ntambi, 1995). Some studies have indicated that SCD-1 is the main isoform and plays a central role in regulation of fatty acid and triglyceride composition in the liver (Miyazaki et al., 2000). Dietary carbohydrates can induce SCD-1 and lipogenic genes in the liver (Sampath and Ntambi, 2011). First, increased insulin secretion by dietary carbohydrate induces lipogenic transcription factors, sterol regulatory element binding protein 1c (SREBP-1c) and liver X receptor (LXR), which can activate transcription of SCD-1 and other lipogenic genes (Chen et al., 2004). Second, increased influx of glucose or fructose to liver can also induce SCD-1 and other lipogenic genes by a SREBP-1c-dependent and -independent mechanism (Miyazaki et al., 2001a, 2004). Therefore, the excess intake of dietary carbohydrate and some kind of fatty acids, or a food condition that increases insulin secretion possibly causes increased liver SCD-1 activity and triglyceride accumulation.

SCD-1 deficiency in the whole body or liver has reduced lipid synthesis and enhanced lipid oxidation, thermogenesis and insulin sensitivity in various tissues including liver, muscle and adipose tissue. These metabolic changes protect SCD-1-deficient mice against a variety of dietary, pharmacological and genetic conditions that promote obesity, insulin resistance and hepatic steatosis (Ntambi et al., 2002; Rahman et al., 2003, 2005; Miyazaki et al., 2007). Additionally, pharmacological inhibition of SCD-1 also improved hepatic lipid accumulation

and metabolic disorders (Issandou et al., 2009; Koltun et al., 2009; Ramtohul et al., 2010). These reports demonstrate that SCD-1 plays a key role in regulating hepatic triglyceride levels and abnormal activation of SCD-1 may lead to hepatic steatosis. In contrast, it is poorly understood how SCD-1 affects the onset of the NASH phenotype including liver injury, inflammation and fibrosis. In this chapter, I evaluated the effects of SCD-1 on onset phase of NASH in rat models using an SCD-1 inhibitor.

Many animal models have been used for NASH/NAFLD research. Obese and type 2 diabetes models such as *ob/ob* mice, *db/db* mice and Zucker fatty rats generally do not lead to liver fibrosis; therefore they are not useful in researching NASH pathology. Actually, some of the NASH/NAFLD models exhibit no or slight fibrosis. Methionine and choline-deficient (MCD) diet models are one of the most useful NASH models and they develop liver fibrosis that is histologically similar to human NASH (Fan and Qiao, 2009). Methionine and choline are used to synthesize phosphatidylcholine, which is necessary for the secretion of triglyceride from the liver to blood as VLDL. Consequently, deficiency in methionine and choline leads to triglyceride accumulation in the liver. Additionally, methionine is a precursor of glutathione, an endogenous antioxidative protein. Deficiency in methionine also causes oxidative stress in liver and subsequently leads to liver injury, inflammation and fibrosis. However, MCD diet models require a long time period (over 3 or 4 months) to exhibit remarkable fibrosis. For efficient *in vivo* screening of drug candidates, the throughput was very important. Therefore, I tried to modify the MCD models to evaluate fibrosis in a shorter period than conventional methods. It has been reported that rat collagen 1a1 promoter-luciferase transgenic (Col1a1-Luc Tg) rats, in which the expression of luciferase is regulated under the native promoter of collagen 1a1, were established. They are appropriate to sensitively evaluate the fibrosis of kidneys and various organs in a short-term period (Terashima et al., 2010). In these rats, the pro-fibrogenic response with altered mRNA expression of collagen 1a1 could be detected even if protein levels of collagen are not sufficiently increased. Furthermore, luciferase is easier to measure than real time RT-PCR analysis; therefore they are useful in *in vivo* screening. In my present

study, Col1a1-Luc Tg rats were used to evaluate the effects of SCD-1 on the onset of NASH including the pro-fibrogenic response in a short-term period.

Materials and Methods

Synthesis of an SCD-1 inhibitor

N-(2-hydroxy-2-phenylethyl)-6-[4-(2-methylbenzoyl)piperidin-1-yl]pyridazine-3-carboxamide (**Figure 3**; page 78), a potent and orally available SCD-1 inhibitor named as compound A, was discovered by Daiichi Sankyo, Co., Ltd. The detailed synthetic procedures, physicochemical properties and pharmacokinetic profile of compound A with this structural motif have been previously reported (Uto et al., 2010).

Animals

All experimental procedures were performed in accordance with the in-house guideline of the International Animal Care and Use Committee of Daiichi Sankyo Co., Ltd. Col1a1-Luc Tg rats were generated by a previously reported method, and bred in Japan SLC Inc. (Shizuoka, Japan) (Terashima et al., 2010). C57BL/6J mice were purchased from Charles River Laboratories Japan, Inc. (Yokohama, Japan). They were maintained in a room under a temperature controlled at 23°C±2 and a 12-hour light-dark lighting cycle. The animals were allowed a standard pellet chow before the experiment and water *ad libitum*. Anesthesia was performed by intraperitoneally injecting pentobarbital (Dainippon Pharmaceutical, Osaka, Japan) at a dose of 50 mg/kg.

Mice fed with lipogenic diets

In order to evaluate liver SCD-1 activity, 9 week old male C57BL/6J mice were fed with non-fat and high-sucrose (lipogenic) diets (Research Diets, Inc., New Brunswich, NJ, USA,) for 7 days prior to administration of compound A. Lipogenic diets were composed of 22 kcal% protein and 78 kcal% carbohydrate as sucrose. Compound A was administered once at doses of 10, 30 and 100 mg/kg (n = 2) to mice by oral gavage in a 4:1 mixture of polypyleneglycol and Tween 80 (PG:Tween) as vehicle. In order to evaluate liver triglyceride content, the mice

were fed with lipogenic diets for 14 days, and compound A was administered once-daily at doses of 10, 30 and 100 mg/kg (n = 6) to mice during the last 7 days of the feeding of lipogenic diets. The mice in the normal group were fed with standard chow diets (FR-2, Funabashi Farm Co., Chiba, Japan). At the next day of the 7th administration of compound A, the mice were sacrificed and the livers were removed and washed with saline. The specimens of liver were immediately snap-frozen and stored at –80°C to measure triglyceride content.

In vivo liver SCD-1 activity

After 6 hours of administration of compound A in mice fed with lipogenic diets, [^{14}C]stearate (Daiichi Pure Chemicals, Tokyo, Japan) dissolved in saline containing 2% bovine serum albumin was intraperitoneally administered at a dose of 100 μL/kg to mice. One hour after the injection of [^{14}C]stearate, the mice were sacrificed under anesthesia and the livers were collected and quickly frozen in liquid nitrogen. The livers were homogenized in 9×volume of cold phosphate buffered-saline (PBS), and 250 μL of homogenates were mixed with an equal volume of methanol containing 10% KOH and then the mixture was saponified at 80°C for 30 min. The free fatty acids in the reaction were protonated by the addition of 5N HCl (15 μL) and extracted with 100 μL ethyl acetate. The 30 μL of the ethyl acetate extracts of each reaction were charged to an $AgNO_3$-TLC plate (20 x 20 cm LK5D plates, 150 Å pore diameter, 250 μm thick) and differentiated in a solvent consisting of chloroform : methanol : acetate : water (90:8:1:0.8). The [^{14}C]stearate and [^{14}C]oleate were quantified with BAS2500 (Fujifilm Corporation, Tokyo, Japan) and SCD-1 activity was determined as the ratio of [^{14}C]oleate to [^{14}C]stearate.

Rats fed with MCD diets

In the first experiments, male Col1a1-Luc Tg rats (184 to 247 g body weight) were randomly divided into four groups as follows:

Group 1: Control sacrificed at 2 weeks (n = 5)

Group 2: MCD sacrificed at 2 weeks (n = 5)

Group 3: Control sacrificed at 8 weeks (n = 5)

Group 4: MCD sacrificed at 8 weeks (n = 5)

Rats in Group 2 and 4 were fed with lipogenic MCD diets (Oriental Yeast Co., Ltd, Tokyo, Japan). Lipogenic MCD diets were composed of 16 kcal% protein (as defined amino acid), 63 kcal% carbohydrate (7:3 sucrose-corn starch) and 21 kcal% fat (as corn oil). Rats in Group 1 and 3 were fed with lipogenic MCD diets supplemented with 3 g/kg of DL-methionine and 2 g/kg of choline bitarate. Rats were sacrificed under anesthesia at 2 weeks in Group 1 and 2, and 8 weeks in Group 3 and 4 after the beginning of the MCD diets, respectively. The livers were removed and washed with saline. The specimens of liver were immediately snap-frozen and stored at –80°C to measure liver lipid and luciferase content.

In the second experiments, male 16 weeks old Col1a1-Luc Tg rats (235 to 282 g body weight) were randomly divided into four groups as follows:

Group 1: Control group (n = 4)

Group 2: MCD group (n = 8)

Group 3: Low dose of compound A group (n = 5)

Group 4: High dose of compound A group (n = 4)

Rats in Group 2, 3 and 4 were fed with lipogenic MCD diets for 8 weeks. Rats in Group 1 were fed with lipogenic MCD diets supplemented with 3 g/kg of DL-methionine and 2 g/kg of choline bitartrate. Compound A dissolved in PG:Tween was administered once-daily at doses of 30 or 100 mg/kg by oral gavage to rats in Group 3 and Group 4 during the feeding of MCD diets, respectively. Rats in Group 1 and 2 were treated with PG:Tween as vehicle. Rats were sacrificed at 8 weeks after starting the administration under anesthesia. Blood was collected from the aorta, and plasma was separated by centrifugation and stored at −80°C. The livers were removed, washed with saline and weighed. The specimens of liver were immediately snap-frozen and stored at −80°C for TaqMan PCR analysis, measurement of liver lipid, luciferase and hydroxyproline content. Portions of the liver lobes were also fixed in 10% buffered formalin (Wako Pure Chemical Industries, Osaka, Japan) and embedded in paraffin for histopathological analysis.

Liver luciferase content

The liver tissues were homogenized by a Polytron homogenizer (Kinematica AG, Luzen, Switzerland) with the addition of 1 mL PBS per 1 g of liver. After centrifugation at 3,000 rpm for 20 min, the luminescence in the supernatant was measured by a PicaGene kit (Toyo Ink MFG Co., Ltd., Tokyo, Japan). The concentration of luciferase was quantified using the standard curve of luciferase protein (Toyo Ink MFG Co.). The protein concentration was measured by a protein assay reagent (Bio-Rad Laboratories, Inc., Tokyo, Japan) , and luciferase was indicated as pg/mg protein.

Liver triglyceride content

A piece of liver was homogenized by Polytron homogenizer (Kinematica AG) with the addition of PBS. The homogenates were mixed with the combination of $CHCl_3$ and MeOH (2:1). After 5 minutes of combining by a vortex mixer, the solutions were centrifuged at 14,000 rpm for 3 min. The lower layers were collected and evaporated. After being dissolved in isopropanol containing 10% Triton, triglyceride content was measured by Triglyceride E test-Wako (Wako Pure Chemical Industries).

Plasma AST and ALT

Aspartate aminotransferase (AST) and alanine aminotransferase (ALT) levels in the plasma were measured using an Autoanalyzer (Hitachi 7250, Hitachi High-Technologies Corporation, Tokyo, Japan).

Real time RT-PCR analysis

The liver tissues were homogenized by a Polytron homogenizer (Kinematica AG) with the addition of Trizol reagent (Invitrogen, Carlsbad, CA). After centrifugation at 10,000 rpm at 25°C, 0.2 mL chloroform was added and mixed by a vortex mixer. After 10 min incubation at room temperature, they were centrifuged at 10,000 rpm at 25°C, and the water layer was collected. RNA was purified by an Rneasy Mini Kit (Qiagen, Valencia, CA) and RNA concentration was measured by Gene Spec III (Hitachi, Tokyo, Japan). cDNA was synthesized by a High Capacity cDNA

Reverse Transcription Kit (Applied Biosystems, Foster City, CA). TaqMan PCR was carried out by ABI PRISM 7900 (PerkinElmer Life Sciences, Boston, MA). The mixture containing 5 μL cDNA, 25 μL TaqMan 2×PCR Master Mix (Applied Biosystems), 0.5 μL forward primer, 0.5 μL reverse primer and 0.5 μL TaqMan probe, were reacted together. The thermal cycler conditions were 2 min at 50°C, 10 min at 95°C, and 40 cycles of 15 sec at 95°C followed by 1 min at 60°C. The fluorescent TaqMan probes and forward and reverse primers were designed with the software Primer Express™, Ver.1.0 (Applied Biosystems, Foster City, CA) and synthesized by Sigma Genosys Japan (Hokkaido, Japan). The sequences of primers and probes used in this study were indicated in **Table 1** (page 71). All the probes contained a fluorescence reporter (6-carboxyfluorescein [*FAM*]) at the 5' end and a fluorescence quencher (6-carboxytetramethylrhodamine [*TAMRA*]) at the 3' end. Rodent GAPDH Control Reagents (Applied Biosystems) were used as an internal standard. Control RNA (Rodent, 50 ng/L) was serially diluted 5-fold with 1×TE (Wako) down to 80 pg/L. The amplification of standard and sample cDNA was carried out in a MicroAmp Optical 96-well reaction plate (Applied Biosystems). All standards and samples were assayed in duplicate. Each plate always contained the same standard. The threshold cycle (*Ct*) values were used to plot a standard curve in which *Ct* decreased in proportion to the log of the template copy number. The correlation coefficients of the standard curves were always more than 99%.

Liver hydroxyproline content

Liver tissue (approximately 400 mg of wet weight) was hydrolyzed in 4 mL of 6 mol/L hydrochloric acid at 105°C overnight. The hydrolysate was centrifuged at 800 g for 15 min and 20 μL of the supernatant was evaporated under vacuum. Then, the sediment was dissolved in 0.6 mL of 50% isopropanol and incubated with 0.1 mL of chloramine-T solution, containing 42 mg of chloramine-T (Wako Pure Chemical Industries) dissolved in 6.9 mL of acetate-citrate buffer and 0.21 mL of distilled water, for 10 min at room temperature. In turn, 0.5 mL of Ehrlich's solution, including 5 g of *p*-dimethylaminobenzaldehyde (Wako Pure Chemical Industries) dissolved in 5.5 mL of 60% perchloric acid, and 26.8 mL isopropanol, were added and incubated at 50°C for 90 min. After cooling, the

absorbance was read at 558 nm. The hydroxyproline concentration was calculated from a standard curve prepared with high-purity hydroxyproline (Wako Pure Chemical Industries). Hydroxyproline levels were expressed in micrograms of hydroxyproline per gram liver.

Histological analysis

Histological analysis was performed in Histo. Science Laboratory Co., Ltd. (Tokyo, Japan) Formalin-fixed liver tissue was embedded in paraffin. Sections were stained with hematoxylin-eosin and Masson-trichrome. The severity was scored by a histopathologist. Hepatocellular degeneration and inflammation were scored as follows: 0, none; 1, slight; 2, mild; 3, moderate. Inflammation was indicated as the sum (0 to 6) of portal inflammation (score: 0 to 3) and lobular inflammation (score: 0 to 3). Fibrosis was indicated as follows: 1, pericellular and perivenular fibrosis; 2, focal bridging fibrosis; 3, bridging fibrosis with lobular distortion; 4, cirrhosis.

Statistical analysis

Results were expressed as the mean ± S.E. Student's t-test (when the F-test was significant, the Welch test was used) and Dunnett's test was used to compare two groups and three or more groups, respectively. The Wilcoxon test was used in histological analysis. $p < 0.05$ was considered statistically significant. The SAS System Release 8.2 (SAS Institute Inc.) was used for the statistical analyses.

Results

Effects of SCD-1 inhibitor on liver SCD-1 activity and triglyceride accumulation in mice fed with lipogenic diets *in vivo*

SCD-1 inhibitors were screened to obtain a research tool compound, and a lead compound reported by Xenon Pharmaceuticals, which had potent *in vitro* activity but low bioavailability, was structurally optimized as previously reported (Uto et al., 2010). As a result, a potent and orally-available SCD-1 inhibitor, compound A, was obtained, in which the 50% of inhibitory concentration was 51 nM.

In order to evaluate *in vivo* liver SCD-1 inhibition of compound A, I used mice fed with lipogenic diets based on high-carbohydrate and non-fat diets. After 7 days feeding of lipogenic diets, compound A was administered to mice in a single oral dosing. Compound A inhibited liver SCD-1 activity in a dose dependent manner (**Figure 4-A**; page 79). The 50% inhibitory dose (ID_{50}) was 17.2 mg/kg. Next, after 7 days feeding of lipogenic diets, compound A was orally administered once daily for 7 days during an additional 7 days feeding of the diets. Liver triglyceride content was increased 2-fold, and repeated dosing of compound A decreased high carbohydrate-induced triglyceride accumulation in the liver in a dose dependent manner (**Figure 4-B**; page 79).

Evaluation of rats fed with MCD diets

In order to evaluate the effects of SCD-1 on NASH pathology, Col1a1-Luc Tg rats were fed with lipogenic MCD diets and the time course of disease was confirmed to fix experimental conditions. Luciferase in the liver, reflecting collagen 1a1-promoter activity, was measured to evaluate a pro-fibrogenic response in the liver of MCD rats. Luciferase in liver of MCD rats was significantly increased by 3.3-fold at 8 weeks compared with control rats, although that at 2 weeks was not significantly increased (**Figure 5-A**; page 80). Liver triglyceride content in MCD rats were significantly increased at 2 and 8 weeks compared with control rats (**Figure 5-B**; page 80). Therefore, in the next study, MCD diets were fed for 8

weeks to rats in order to evaluate the effects of the SCD-1 inhibitor.

Effects of SCD-1 on body weight change and liver weight in MCD rats

In order to evaluate the effects of SCD-1 in the onset phase of NASH, Col1a1-Luc Tg rats were fed with lipogenic MCD diets for 8 weeks. SCD-1 inhibitor, compound A was administered once-daily to rats at doses of 30 and 100 mg/kg/day. The MCD diets caused body weight loss of 30% in the rats (**Table 2**; page 72). The treatment of the SCD-1 inhibitor did not affect the body weight change in rats fed with MCD diets. Neither MCD diets nor treatment of SCD-1 inhibitor significantly affected relative liver weight in MCD rats.

Effects of SCD-1 on liver lipid accumulation in MCD rats

In order to evaluate the effects of SCD-1 on liver triglyceride accumulation, the first process of NASH/NAFLD, liver triglyceride levels were evaluated. MCD diets increased triglyceride content in the livers of MCD rats by 12-fold, indicating remarkable lipid accumulation in the liver (**Figure 6**; page 81). A high dose of SCD-1 inhibitor significantly reduced triglyceride accumulation in the liver of MCD rats by 80%. These results indicate that SCD-1 is important in regulating liver triglyceride levels and its up-regulation may lead to the development of hepatic steatosis in MCD rats.

Effects of SCD-1 on liver injury in MCD rats

Next, I evaluated the effects of SCD-1 on phenotypes of NASH including liver injury, inflammation and fibrosis. In order to evaluate the effects of SCD-1 in liver injury, plasma markers, AST and ALT were measured. MCD diets increased the plasma AST and ALT levels by 3.3 and 5.5-fold, respectively (**Figure 7**; page 82) SCD-1 inhibitor at doses of 30 and 100 mg/kg/day prevented AST elevation by 75% and 86%, respectively. Treatment of SCD-1 inhibitor at doses of 30 and 100 mg/kg/day also prevented ALT elevation by 66% and 78%, respectively. These results indicate that the SCD-1 inhibitor prevents onset of liver injury after development of hepatic steatosis in MCD rats.

Effects of SCD-1 on histological changes including steatosis, hepatocellular degeneration and inflammation in liver of MCD rats

I evaluated the effects of SCD-1 on histopathology in NASH by hematoxylin-eosin staining. MCD diets initiated severe steatosis in the liver of rats, which was detected as lipid droplets within hepatocytes, although it was not detected in the control group (**Figure 8-A** and **8-B**; pages 83 and 84). Treatment of SCD-1 inhibitor attenuated development of steatosis, shown as a reduction of lipid droplets in the liver, and it was remarkable in the high dose of the SCD-1 inhibitor group (**Figure 8-C** and **8-D**; pages 83 and 84). Hepatocellular degeneration shown as ballooning or necrosis was also observed in the liver of rats fed with MCD diets, and administration of SCD-1 inhibitor attenuated the severity (**Figure 9-A**; page 85). Inflammatory cell infiltration was also observed in the liver of MCD rats, and it was rarely observed in a high dose of the SCD-1 inhibitor group (**Figure 8-E** and **8-F**; pages 83 and 84, **Figure 9-B**; page 85). These results demonstrate that the SCD-1 inhibitor prevents the onset of crucial histopathological changes including hepatic steatosis, hepatocellular degeneration and inflammatory cell infiltration in MCD rats; therefore SCD-1 possibly contributes to NASH pathology including liver injury, inflammation as well as hepatic steatosis.

Effects of SCD-1 on early fibrosis in the liver of MCD rats

In order to evaluate the effects of SCD-1 on liver fibrosis, liver histology was evaluated by Masson-trichrome staining. Slight or mild fibrosis was observed in the liver of MCD rats (**Figure 10-A**; pages 86 and 87). Treatment of SCD-1 inhibitor attenuated the development of these early fibrogenic changes (**Figure 10-B** and **C**; pages 86 and 87). Col1a1-Luc Tg rats were used to evaluate the effects on fibrosis easily and with the short-term period, and in the first study, luciferase in the liver was significantly increased after 8 weeks feeding of MCD diets as shown in **Figure 5-A** (page 80). Unfortunately, the luciferase in this study was not significantly changed in the liver of MCD rats although it showed tendency to increase (**Figure 11-A**; page 88). I suppose that fibrogenic change was

histologically very mild at 8 weeks feeding of MCD diets; therefore it failed to detect in luciferase. Hydroxyproline content, reflecting collagen protein levels, was also not increased in the liver of MCD rats (**Figure 11-B**; page 88). These results indicate that the SCD-1 inhibitor histologically prevents onset of early fibrosis in MCD rats, although it is necessary to study for longer time periods in order to fully evaluate the effects on more established liver fibrosis.

Effects of SCD-1 on mRNA expression of MCP-1 in the liver of MCD rats

Monocyte chemotactic protein-1 (MCP-1) is a key pro-inflammatory cytokine, which is concerned with various inflammatory responses including the liver disease. I evaluated the effects of SCD-1 on mRNA levels of MCP-1 in the liver of MCD rats by real time RT-PCR analysis. The mRNA levels of MCP-1 was drastically increased in the liver of MCD rats (**Figure 12**; page 89). A high dose of SCD-1 inhibitor significantly reduced the mRNA expression.

SCD-1 mRNA expression in liver of MCD rats

I evaluated the effects of MCD diets on mRNA levels of SCD-1 by real time RT-PCR analysis. SCD-1 mRNA levels were remarkably decreased in the livers of MCD rats compared with those of control rats (**Figure 13**; page 90). Its down-regulation is possibly due to protection against rapid triglyceride accumulation resulting from methionine and choline deficiency in the liver.

Discussion

In this chapter, I demonstrated that SCD-1 has a key role in liver lipid accumulation and subsequent onset of liver injury, inflammation and fibrosis in NASH. I used a potent and orally-available SCD-1 inhibitor, compound A, obtained by lead optimization as previously reported (Uto et al., 2010). In order to measure the *in vivo* inhibitory activity of compound A to liver SCD-1, mice were fed with lipogenic diets based on high-carbohydrate and non-fat that up-regulate SCD-1 activity in the liver (Flowers et al., 2006, 2008). A single oral administration of compound A inhibited SCD-1 activity in the liver of mice fed with lipogenic diets. Liver triglyceride content was increased by 2-fold in the liver of mice fed with lipogenic diets for 14 days compared with standard chow diets. Repeated administration of the SCD-1 inhibitor for 7 days completely inhibited lipogenic diet-induced triglyceride accumulation in the liver.

My results are consistent with previous reports in SCD-1 deficient mice and pharmacological inhibition which were protective against triglyceride accumulation in the liver after feeding of lipogenic diets (Miyazaki et al., 2001a; Issandou et al., 2009). All of these previous reports used metabolic syndrome models with obesity and insulin resistance. I used NASH models to evaluate the effects of an SCD-1 inhibitor for the first time. In NASH rats fed with lipogenic MCD diets, SCD-1 inhibitor also inhibited triglyceride accumulation in the liver as well as metabolic syndrome models. Buque et al. reported that SCD-1 expression levels were significantly correlated with the severity of fatty liver in obese rats (Buque et al., 2010). In human study, liver SCD-1 activities were also higher in obese patients with fatty liver than in those without fatty liver, and they were related to the percentage of liver fat (Kotronen et al., 2009). My results and these other reports suggest that SCD-1 plays a key role in regulating liver lipid levels in metabolic disorders including NASH/NAFLD. Liver specific disruption of SCD-1 as well as deficiency in the whole body was protective against lipid accumulation in the liver (Ntambi et al., 2002; Miyazaki et al., 2007). These

reflect that liver SCD-1 importantly regulates liver lipid levels. Interestingly, skin-specific disruption of SCD-1 but not adipose-specific one also protected against lipid accumulation in the liver by increasing fatty acid oxidation (Sampath et al., 2009; Flowers et al., 2012). In skin-specific deficiency of SCD-1, hepatic lipogenic response to high-carbohydrate diets were intact. In addition to liver, SCD-1 in skin and other organs possibly affects the development of hepatic steatosis in NASH/NAFLD in unknown ways other than increased hepatic lipogenesis.

Recent studies have focused on the involvement of SCD-1 in the development of hepatic steatosis; however there is little information about the contribution of SCD-1 to the development of NASH pathology. Therefore, I evaluated the effects of SCD-1 on the onset of NASH phenotypes including liver injury, inflammation and fibrosis. This is the first report that SCD-1 inhibition attenuated these pathology of NASH. MCD diets histologically developed hepatocellular degeneration and inflammatory cell infiltration in the liver of rats. Importantly, treatment of SCD-1 inhibitor attenuated these pathological observations in addition to plasma biomarkers of liver injury, AST and ALT in rats fed with MCD diets. MCP-1 is a pro-inflammatory cytokine and concerned with various inflammatory diseases including liver disease. In chronically injured liver including NASH, activated HSCs, key players in liver fibrosis, proliferate and continuously produce collagen. Additionally, activated HSCs also induce chemotaxis and activation of inflammatory cells such as monocytes/macrophages and T lymphocytes by production of inflammatory cytokines such as MCP-1 (Marra et al., 1993; Czaja et al., 1994). HSCs can also migrate towards these cytokine chemoattractants (Marra et al., 1999). It was reported that the feeding of MCD diets to mice increased mRNA expression of MCP-1 in the liver (Zhang et al., 2009). In my present study, the mRNA expression of MCP-1 was also increased in the liver of rats fed with MCD diets. Treatment of SCD-1 inhibitor attenuated the MCD diets-induced MCP-1 up-regulation in the liver of rats. These results suggest that SCD-1 inhibition decrease sensitivity of the liver to pathogenesis of NASH including liver injury and inflammation after development of hepatic steatosis.

It was previously reported that Col1a1-Luc Tg rats were useful as fibrosis models of the kidney and other organs, in which organ fibrosis was evaluated easily and in a short-term period (Terashima et al., 2010). In my present study, Col1a1-Luc Tg rats were used to evaluate pro-fibrogenic responses in livers of rats fed with MCD diets in a short-term period. In the first study to confirm experimental conditions, luciferase, reflecting collagen 1a1 promoter activity, in the liver was significantly increased after 8 weeks MCD diets. In the next study, the luciferase also showed a tendency to increase in rats fed with MCD diets for 8 weeks, although it was not significant. The liver hydroxyproline levels, reflecting protein levels of collagen, also showed no changes in MCD rats. Therefore, to fully evaluate the effects on established fibrosis in these methods, a longer time period may be necessary. In contrast, histological analysis showed slight or mild fibrosis in the liver of MCD rats, and treatment of SCD-1 inhibitor prevented the onset of the early fibrosis. These results support that SCD-1 plays a key role in the onset of NASH pathology including liver injury, inflammation and early fibrosis.

Interestingly, SCD-1 inhibitor decreased triglyceride accumulation in the liver only in treatments with a high dose, but the liver injury, inflammation and early fibrosis were attenuated even in a low dose. I suppose that levels of triglyceride, which are a storage form of lipids, are not so important and those of free fatty acid cause liver injury and other pathology with NASH. Fatty acids are key mediators for hepatocyte lipotoxicity, and play a role in hepatocellular death, oxidative and endoplasmic reticulum stress, inflammation and fibrosis (Trauner et al., 2010). MUFAs are thought to be less toxic than saturated fatty acids, and it was reported that MUFAs protected cells against saturated fatty acids-induced apoptosis (Eitel et al., 2002). From this point of view, SCD-1 inhibition could increase the toxicity of fatty acids because SCD-1 activity could result in increased MUFAs and decreased saturated fatty acids. Unbalanced accumulation of saturated fatty acids resulting from decrease of SCD-1 were reported in the liver of mice fed with MCD diets, suggesting that depletion of MUFAs contribute to liver injury (Eitel et al., 2002). Furthermore, Li et al. reported that MCD diets in SCD-1 deficient mice increased hepatocellular apoptosis, liver injury and fibrosis although hepatic steatosis was ameliorated (Li et al., 2009). They suggested that

liver SCD-1 plays a key role in the prevention of liver injury by safely converting toxic fatty acids to MUFAs. In contrast, my results indicate that SCD-1 inhibition is protective against inflammation and liver injury in rats fed with MCD diets. Larter et al. reported that feeding of MUFA-rich diets did not prevent MCD diet-induced liver injuries in spite of an increased ratio of MUFAs in liver fatty acids (Larter et al., 2008). They suggested that accumulation of fatty acids *per se* may be important in liver injury, and it was not dependent on the nature of the fatty acid source. It was also reported that saturated fatty acids and MUFAs have similar effects on sensitization to TRAIL-induced apoptosis in cells (Malhi et al., 2007). In human NASH, both saturated fatty acids and MUFAs are accumulated in the liver (Puri et al., 2007). These reports and our results show that MUFAs as well as saturated fatty acids also play a role in liver injury in NASH. One possible explanation for opposite results by Li et al. as described above is that toxicity by systemic inhibition of SCD-1 may contribute to SCD-1 deficiency-induced exacerbation of liver injury. It was recently reported that SCD-1 also seems to be concerned with inflammation in some organs (Liu et al., 2011). SCD-1 inhibitor did not cause inflammation; however other compounds with more potent systemic inhibition of SCD-1 increased white blood cells (Uto et al., 2011). Importantly, these potent compounds reduced the beneficial effects on plasma triglyceride levels. These findings show that toxic effects of systemic inhibition of SCD-1 possibly cancel the beneficial effects. Another explanation is the differences between genetic disruption and pharmacological inhibition. Inborn and complete deficiency of SCD-1 with genetic disruption might be not applicable to evaluate the pathology of NASH because environmental and life style related factors are involved in most of the elderly patients.

Liver lipid levels are mainly regulated by four processes such as fatty acid uptake into the liver, *de novo* lipogenesis, VLDL secretion from the liver and fatty acid oxidation. In human obesity with NAFLD, the main mechanism of liver lipid accumulation is possibly due to increased fatty acid uptake and *de novo* lipogenesis caused by insulin resistance. In contrast, MCD diets induce liver triglyceride accumulation by mainly decreased triglyceride secretion from the liver as VLDL and increased fatty acid uptake (Rinella et al., 2008). In my present

study, mRNA expression of SCD-1 in the liver of rats fed with MCD diets was also remarkably decreased as previously reported in mice fed with MCD diets (Rizki et al., 2006). Triglyceride accumulation in the liver is much more rapid in those fed with MCD diets than general lipogenic diets containing normal levels of methionine and choline. Therefore, one possible explanation is that down-regulation of SCD-1 after feeding of MCD diets may be a protective mechanism against rapid triglyceride accumulation. Importantly, the SCD-1 inhibitor effectively inhibited liver triglyceride accumulation in rats fed with MCD diets in spite of a remarkably decreased mRNA expression of SCD-1 and also presumably decreased the enzymatic activity. I suppose that SCD-1 inhibition decreased liver triglyceride accumulation in MCD rats resulting from a change of balance in these processes of fatty acid metabolism in the liver, although the contribution of SCD-1 might be reduced in these models compared with human patients. It is known that generally used lipogenic diets such as high-fat or high-carbohydrate or insulin resistant/diabetic animals such as *ob/ob*, *db/db* or ZDF cause hepatic steatosis but no steatohepatitis with fibrosis; therefore I used MCD diet models in my present study although SCD-1 expression showed an opposite change. It was recently reported that long-term feeding of cholesterol-containing atherogenic diets to mice induced liver injury, inflammation and fibrosis, in which induced SCD-1 expression through dietary cholesterol-induced LXR activation and subsequent increased hepatic lipogenesis were involved (Matsuzawa et al., 2007). I suppose potent beneficial effects of SCD-1 inhibitors in such SCD-1 up-regulated NASH models.

In summary, an SCD-1 inhibitor prevented hepatic steatosis and subsequent pathology including liver injury, inflammation and fibrosis in NASH (summarized in **Figure 14**; page 91). These results demonstrate that SCD-1 plays an important role in the onset process of NASH.

Chapter II

“Effects of angiotensin II on the progression of liver fibrosis”

Introduction

Ang II is a major component of renin-angiotensin systems (RAS), which contain angiotensinogen, renin, angiotensin I, angiotensin-converting enzyme (ACE) and Ang II receptors. Ang II and RAS play central roles in the regulation of systemic blood pressure and fluid homeostasis by vasoconstriction of smooth muscle cells and sodium retension (Brewster et al., 2003). In addition to these “systemic RAS”, “local RAS” are regulated within individual organs including the liver and is thought to play an important role in the local response to disease (Paul et al., 2006). The action of Ang II is mainly mediated by two subtypes of receptors, angiotensin II type 1 (AT1) and type 2 (AT2) receptors, which are distributed in many kinds of organs and tissues. The action of Ang II primarily is mediated by AT1 receptor (Mehta and Griendling, 2007). AT2 receptor generally have divergent pathways compared with AT1 receptor.

Several lines of evidence have suggested that RAS also plays an important role in the pathogenesis of organ fibrosis (Brilla, 2000; Sun et al., 2000). In mesangial cells and other cell types, Ang II has been shown to promote the proliferation and collagen synthesis (Ray et al., 1991; Wolf et al., 1992; Kagami et al., 1994; Weber et al., 1994; Tharaux et al., 2000). Additionally, the expression of TGF-β1, the key cytokine in the development of cardiac and renal fibrosis, is increased by Ang II (Weber, 1997). Blockade of RAS with ACE inhibitors or angiotensin receptor blockers (ARBs) has been shown to ameliorate the progression of organ fibrosis (Ishidoya et al., 1995; Kim et al., 1995; Molteni et al., 2000).

In the liver, Ang II is considered to regulate intrahepatic circulation (Schneider et al., 1999). It has been also reported that Ang II induces proliferation and contraction of human HSCs, key players in liver fibrosis (Bataller et al., 2000). Additionally, ACE inhibitors or ARBs were shown to attenuate the progression of liver fibrosis *in vivo* (Ramos et al., 1994; Jonsson et al., 2001; Ohishi et al., 2001; Paizis et al., 2001; Yoshiji et al., 2002). These reports suggested that Ang II and

RAS might play an important role in the pathogenesis of liver fibrosis including NASH. However, the precise molecular mechanism of Ang II-mediated liver fibrosis and activation of HSCs were poorly understood.

Bile duct ligation (BDL) is generally used as liver fibrosis models. BDL stimulates proliferation of bile duct epithelial cells and finally causes portal inflammation and fibrosis (Peter, 2011). BDL model does not show hepatic steatosis and related metabolic disorders, and are pure fibrosis models. It was reported that key elements of RAS including ACE and AT1 receptors were up-regulated in the liver of BDL rats, indicating possible contribution of RAS to fibrosis in the model (Paizis et al., 2002). The comparison of BDL model with MCD model used in "Chapter I" is 1 in **Table 3** (page 73). In my present study, I used BDL models to purely evaluate progression of liver fibrosis, although it is necessary to evaluate in MCD models.

Olmesartan medoxomil (olmesartan), (5-methyl-2-oxo-1,3-dioxolen -4-yl) methoxy-4-(1-hydroxy-1-methylethyl)-2-propyl-1-{4-[2-(tetrazol-5-yl)-phenyl] phenyl}methylimidazol-5-carboxylate, is a potent ARB and is commercially used as an antihypertensive agent globally. Olmesartan is a prodrug containing an ester moiety which is rapidly cleaved to release the active form of olmesartan, RNH-6270, after oral administration (Mizuno et al., 1995). Chemical structures of olmesartan and RNH-6270 were shown in **Figure 15** (page 92).

In this chapter, in order to elucidate the molecular mechanism of Ang II-mediated liver fibrosis progression, I evaluated the effects of Ang II on *in vivo* liver fibrosis models and *in vitro* activated HSCs using ARB, olmesartan.

Materials and Methods

Synthesis of olmesartan and RNH-6270

Olmesartan and its active metabolite, RNH-6270 were discovered and synthesized in Sankyo Co., Ltd.

Animals

All animal experiments were performed in accordance with the Animal Experimentation Guidelines of Sankyo Co., Ltd. Sprague-Dawley (SD) male rats were purchased from Japan SLC Inc. (Shizuoka, Japan), and maintained in a room under a temperature controlled at 23°C ± 2 and a 12-hour light-dark lighting cycle. The animals were allowed a standard pellet chow and water *ad libitum*. Anesthesia was performed by intraperitoneally injecting pentobarbital (Dainippon Pharmaceutical) at a dose of 50 mg/kg.

Rats with common bile duct ligation

Liver fibrosis was induced by common bile duct ligation, as previously described (Kountouras et al., 1984). SD male rats (200 to 250 g body weight) were used. The common bile duct was double-ligated and cut between the ligatures. In the first experiment, some rats received BDL and others received a sham-operation, in which they were subjected to a midline incision and manipulation of the common bile duct without ligation. Rats were divided into six groups and sacrificed at indicated times (1 to 3 weeks) after surgery under anesthesia as follows:

Group 1: Sham sacrificed at 1 week (n =3)

Group 2: BDL sacrificed at 1 week (n = 3)

Group 3: Sham sacrificed at 2 weeks (n = 5)

Group 4: BDL sacrificed at 2 weeks (n = 6)

Group 5: Sham sacrificed at 3 weeks (n = 5)

Group 6: BDL sacrificed at 3 weeks (n = 5)

In the second experiment, rats were divided into three groups at 7 days after

surgery as follows:

Group 1: Sham group (n = 5)

Group 2: BDL group (n = 10)

Group 3: BDL + ARB group (n =10)

In Group 3, olmesartan, dissolved in a solution of 0.5% carboxymethyl cellulose (CMC, Nacalai Tesque, Kyoto, Japan), was orally administered at a dose of 1 mg/kg six times a week from 7 days to 20 days after the surgery. In Group 1 and 2, rats received the vehicle for the same time period. Rats were sacrificed at 21 days after surgery under anesthesia. Blood was collected from the aorta, and plasma was prepared by centrifugation. Plasma samples were frozen and stored at –80°C. The livers were washed with saline and weighed. The specimens of liver were immediately snap-frozen and stored at –80°C for real time RT-PCR analysis and measurement of hydroxyproline content. Portions of liver lobes were also fixed in 10% buffered formalin (Wako Pure Chemical Industries) and embedded in paraffin for histological analysis.

Liver hydroxyproline content

Liver tissue (approximately 400 mg of wet weight) was hydrolyzed in 4 mL of 6 mol/L hydrochloric acid at 105°C overnight. The hydrolysate was centrifuged at 800 g for 15 min and 20 μL of the supernatant was evaporated under vacuum. Then, the sediment was dissolved in 0.6 mL of 50% isopropanol and incubated with 0.1 mL of chloramine-T solution, containing 42 mg of chloramine-T (Wako Pure Chemical Industries) dissolved in 6.9 mL of acetate-citrate buffer and 0.21 mL of distilled water, for 10 min at room temperature. In turn, 0.5 mL of Ehrlich's solution, including 5 g of *p*-dimethylaminobenzaldehyde (Wako Pure Chemical Industries) dissolved in 5.5 mL of 60% perchloric acid, and 26.8 mL isopropanol, were added and incubated at 50°C for 90 min. After cooling, the absorbance was read at 558 nm. The hydroxyproline concentration was calculated from a standard curve prepared with high-purity hydroxyproline (Wako Pure Chemical Industries). Hydroxyproline levels were expressed in micrograms of hydroxyproline per gram liver.

Plasma AST and ALT

AST and ALT levels in the plasma were measured using an Autoanalyzer (Hitachi 7250, Hitachi High-Technologies Corporation).

Histological analysis

Liver sections were incubated with xylene and hydrated through several washes in ethanol and distilled water to remove the paraffin. The sections were either stained with Masson-trichrome or subjected to immunohistostaining using antibodies against α-SMA or AT1 receptor. For AT1 immunohistostaining, sections were heated with 10 mmol/L sodium citrate buffer (pH 6.0) at 120°C for 10 min. Endogenous peroxidase activity was quenched by the addition of 3%(v/v) hydrogen peroxide for 5 min. Unspecific binding sites were blocked by Block Ace (Dainippon Pharmaceutical) for 30 min. Polyclonal anti-rabbit AT1 (Santa Cruz Biotechnology, Santa Cruz, CA) diluted 1:200 in Block Ace was used. The sections were incubated for 30 min with the primary antibody at room temperature, the secondary antibody (goat anti-rabbit IgG, biotinylated, Santa Cruz; diluted 1:100 in Block Ace) for 30 min, and finally, with peroxidase-conjugated streptavidin (Nichirei, Tokyo, Japan). For α-SMA immunohistostaining, after endogenous peroxidase inactivation, sections were incubated for 60 min with mouse monoclonal anti-human smooth muscle actin/HRP (DAKO Japan, Kyoto, Japan) at room temperature. The immunoreactivity was detected by the addition of 3,3'-diaminobenzidine tetrahydrochloride (DAB, DAKO Japan) at room temperature. Between each step, the sections were washed three times with tris-buffered saline (TBS, DAKO Japan) for 5 min. The sections were counterstained with Carazzi's hematoxylin (Muto Pure Chemicals, Tokyo, Japan), dehydrated and mounted.

Isolation of rat hepatic stellate cells

Rat HSCs were prepared from SD male rats (>500 g body weight) using the method of Kawada et al. with some modifications (Kawada et al., 1998). The liver was perfused through the portal vein with Ca^{2+}- and Mg^{2+}-free Hanks' balanced

salts solution (HBSS; Sigma Chemical Co., St. Louis, MO) containing 0.06% EGTA at a flow rate of 10 mL/min at 37°C for 10 min. The liver was then perfused with HBSS containing 0.1% pronase E (Merck, Damstadt, Germany), followed by 0.02% pronase E and 0.125% collagenase (type IV; Sigma). After perfusion, the digested liver was excised, minced, and incubated with gentle stirring in HBSS containing 0.05% pronase E, 0.05% collagenase, 20 μg/mL Dnase I (Roche Diagnostics, Mannheim, Germany) for 30 min at pH 7.3. After passage through a mesh with a pore size of 150 μm in diameter, the cells were centrifuged twice at 400 g in Gey's balanced salts solution (GBSS) at 4°C for 7 min. The HSC-enriched fraction was obtained by centrifugation in GBSS containing 8.2% Nycodenz (Daiichi Pure Chemicals) at 1,400 g for 20 min. The HSCs in the upper white layer were washed twice by centrifugation. The cells were cultured in Dulbecco's modified Eagle medium (DMEM; Gibco BRL, Grand Island, NY) containing 10% fetal calf serum (FCS), 100 μg/mL gentamicin sulfate (Gibco BRL), 100 μg/mL streptomycin sulfate and 100 units/mL penicillin G sodium (Gibco BRL) on 96-well or 6-well tissue culture plates (FALCON, Beckton Dickinson, Franklin Lakes, NJ) at 37°C under a 5% CO_2 atmosphere. The culture medium was replaced at 2 days after plating and then every 2 to 3 days. Before reaching confluence, the cells were used in each experiment.

Cell proliferation

The proliferation rate of HSCs was determined by measuring the amount of [^{3}H]-thymidine incorporated into the cellular DNA. The media were replaced with serum-free DMEM containing angiotensin II (human, Sigma) with or without RNH-6270 and then pulsed for 48 hrs with 0.5 μCi/mL [methyl-^{3}H]-thymidine (Daiichi Pure Chemicals). At the end of the pulsing period, the plates were frozen and stored at –80°C. After thawing, the cells were incubated with 0.05% trypsin/0.53 mmol/L EDTA solution (Gibco BRL) at 37°C. Cellular DNA was then fixed on a glass filter (Filtermat A, PerkinElmer Inc., Waltham, MA) using a cell harvester (Harvester 96, Hamden, CT). The radioactivity was measured by a liquid scintillation counter (Betaplate 1205, PerkinElmer Inc.).

Collagen synthesis

The rate of collagen synthesis in HSCs was determined by measuring the amount of [^{3}H]-proline incorporated into collagenase-digestible macromolecules. The media were replaced with Ang II in serum-free DMEM containing 0.5 mmol/L 3-aminopropionitrile (Tokyo Kasei Kogyo, Tokyo, Japan) and 0.1 mmol/L L-ascorbic acid (Sigma) in the presence or absence of RNH-6270, and then pulsed for 48 hrs with 0.5 μCi/mL L-[2,3,4,5-^{3}H]-proline (Daiichi Pure Chemicals). At the end of the pulsing period, the plates were frozen and stored at –80°C. After thawing, the cells were precipitated twice with 10% trichloroacetic acid (TCA; Nacalai Tesque, Kyoto, Japan) by centrifugation and washed twice with ethanol-ether (3:1) mixture. After drying overnight, the pellet was digested with 5 mg/mL collagenase type VII (Sigma), dissolved in 50 mmol/L Tris-HCl, and 5 mmol/L $CaCl_2$, at pH 7.4, and at 37°C for 90 min, and precipitated twice with 10% TCA and 5% tannic acid (Sigma) by centrifugation. The supernatants from the two centrifugations were pooled, and 50 μL of the mixture was placed on a Deepwell LumaPlate (PerkinElmer Inc.). After drying overnight, the radioactivity was counted by a microplate scintillation counter (TopCount HTS, PerkinElmer Inc.).

Measurement of TGF-β1

In the *in vitro* experiments, HSCs were incubated with Ang II in the presence or absence of RNH-6270 or platelet-derived growth factor-BB (PDGF-BB, rat; R&D Systems, Minneapolis, MN), which is a homodimer of PDGF-B chain subunit and the most potent mitogen for HSCs, for 48 hrs. Culture supernatants were collected, frozen and stored at –80°C. In order to quantify total TGF-β1, the supernatants were treated with 1 mol/L HCl for 10 min to convert the latent form of TGF-β1 to the active form and neutralized with 1.2 mol/L NaOH and 0.5 mol/L HEPES. In the *in vivo* experiments, plasma samples were treated with 2.5 mol/L acetic acid for 10 min and neutralized with 2.7 mol/L NaOH and 1 mol/L HEPES. The activated samples were measured using TGF-β1 Human, Biotrak ELISA System (Amersham Biosciences, Piscataway, NJ) according to the manufacturer's instructions.

Real time PCR analysis

In the *in vitro* experiments, HSCs were incubated with Ang II in the presence or absence of RNH-6270 for 24 hrs. and total cellular RNA was isolated after lysis of the cells. In the *in vivo* experiments, total RNA was isolated from homogenates of whole livers at Day 21 after surgery. RNA extraction was performed using TRIZOL reagent (Gibco BRL) according to the manufacturer's instructions. RNA purity and concentration were determined using a spectrophotometer (DU 7500, Beckman Coulter, Inc., Brea, CA). Total RNA was converted to complementary DNA (cDNA) with TaqMan Reverse Transcription Reagents (Applied Biosystems) using GeneAmp PCR System 9600 (PerkinElmer Inc.). For cDNA synthesis, 5 μg total RNA, 10 μL 10×RT buffer, 22 μL $MgCl_2$ (25 mM), 20 μL dNTPs mixture (10 μM each), 5 μL random hexamers (50 μM), 2 μL RNase inhibitor (20 U/μL), and 2.5 μL (50 U/μL) Moloney Murine Leukemia Virus Reverse Transcriptase were added to make a total volume of 100 μL. Samples were incubated at 25°C for 10 min and 48°C for 30 min. Reactions were stopped by heating to 95°C for 5 min. The fluorescent TaqMan probes, and forward and reverse primers were designed with the software, Primer Express™, Ver.1.0 (Applied Biosystems, Foster City, CA), and synthesized by Sigma Genosys Japan (Hokkaido, Japan). Sequences of primers and probes used in this study are shown in **Table 1** (page 71). I used a probe and primers from the Rodent GAPDH Control Reagents (Applied Biosystems) for internal calibration. Two-step PCR was carried out using an ABI PRISM 7700 Sequence Detector System (PerkinElmer Inc.). PCR conditions were as follows: 5 μL cDNA solution, 25 μL TaqMan 2×PCR Master Mix (Applied Biosystems), 0.5 μL forward primer (10 μM), 0.5 μL reverse primer (10 μM), and 0.5 μL probe (20 μM) were added to make a total volume of 50 μL. The thermal cycler conditions were 2 min at 50°C, 10 min at 95°C, and 40 cycles of 15 sec at 95°C followed by 1 min at 60°C. Standard curves to determine the mRNA content were generated using the GAPDH control. Control RNA (Rodent, 50 ng/L) was serially diluted 5-fold with 1×TE (Wako) down to 80 pg/L. The amplification of standard and sample cDNA was carried out in a MicroAmp Optical 96-well

reaction plate (Applied Biosystems). All standards and samples were assayed in duplicate. Each plate always contained the same standard. The threshold cycle (*Ct*) values were used to plot a standard curve in which *Ct* decreased in proportion to the log of the template copy number. The correlation coefficients of the standard curves were always more than 99%.

Statistical analysis

Results were expressed as the mean ± S.E. Student's t-test (when the F-test was significant, the Welch test was used) and Dunnett's test was used to compare two groups and three or more groups, respectively. $p < 0.05$ was considered statistically significant. The SAS System Release 8.2 (SAS Institute Inc.) was used for the statistical analyses.

Results

Time course evaluation of *in vivo* liver fibrosis models with BDL

I used BDL model as *in vivo* liver fibrosis models. In order to confirm experimental conditions in BDL rats, the time course of disease progression was evaluated up to 3 weeks after BDL. Liver hydroxyproline content, reflecting collagen protein levels, was increased by 1.9-fold at 1 week after BDL compared with sham-operated rats (**Figure 16**; page 93). Liver hydroxyproline content at both 2 and 3 weeks increased by 2.5-fold. Plasma AST levels at 1, 2 and 3 weeks increased by 3.0, 3.1 and 4.0-fold in BDL rats compared with Sham rats, respectively (**Figure 17**; page 94). In contrast, plasma ALT levels were not significantly changed. Body weight in BDL rats was remarkably decreased for the first 4 days after BDL presumably due to surgical complications although no animals died (**Figure 18**; page 95). In the next study, fibrosis was evaluated at 3 weeks after surgery, and the treatment of compounds started at 7 days after surgery considering surgical damage.

Effects of Ang II on survival rate, body weight change and liver weight in BDL rats *in vivo*

In order to evaluate the effects of Ang II on liver fibrosis *in vivo*, ARB, olmesartan was orally administered at a dose of 1 mg/kg starting at 7 days after BDL. However, two animals in the BDL group and three animals in the ARB-treated group died up to Day 11 after BDL presumably due to surgical complications. The survival rate was not statistically different between these two groups (Fisher's exact test). Final body weight was significantly lower than those in the BDL group compared with the Sham group, but ARB treatment did not significantly affect them (**Table 4**; page 74). The ratio of liver weights to body weights increased in the BDL group by 1.8-fold, which is presumably due to inflammation and fibrosis. It was significantly lower in the ARB-treated group compared with the BDL group.

Effects of Ang II on liver fibrosis in BDL rats *in vivo*

I evaluated the effects of Ang II on liver fibrosis in BDL rats *in vivo*. First, collagen levels were measured as hydroxyproline content in the livers of BDL rats. Liver hydroxyproline content in the BDL group increased by 1.8-fold compared with the Sham group, indicating development of fibrosis (**Figure 19**; page 96). ARB treatment decreased collagen accumulation by 45%. These results suggest that Ang II mediates progression of liver fibrosis in BDL rats through activation of AT1 receptors.

Histological analysis was performed in the liver of BDL rats. Bile duct proliferation was remarkable in the livers of the BDL group resulting from cholestasis after BDL, and it was minimal in the ARB group (**Figure 20-A**; page 97). Masson-trichrome staining showed that collagen deposition spread from the area of bile duct proliferation in the BDL liver, and ARB treatment decreased the area of fibrosis (**Figure 20-A**; page 97). These observations were consistent with the results in liver hydroxyproline content, indicating ARB ameliorated liver fibrosis in BDL rats. Activated HSCs are key players in liver fibrosis and continuously produce collagen and ECMs. Therefore, in order to identify activated HSCs in the BDL liver, immunostaining for α-SMA, a marker protein of activated HSCs, was performed. The number of α-SMA-positive cells, indicating activated HSCs, were remarkably increased in the liver of BDL rats compared with the Sham group (**Figure 20-B**; page 97). These cells were localized in the area of collagen deposition. ARB treatment reduced the number of α-SMA-positive cells in the liver of ARB group. Next, in order to identify expression and distribution of AT1 receptors, immunostaining for AT1 receptor was performed. AT1 receptors were highly expressed in the livers of BDL rats and almost not in the Sham group (**Figure 20-C**; page 97). Importantly, AT1 receptors were localized in the area of collagen deposition and accumulation of α-SMA-positive cells. ARB treatment reduced AT1 receptor positive-cells. These results suggest that activated HSCs expressing AT1 receptors may have a key role in the development of liver fibrosis with stimulation of Ang II in the liver.

Next, I evaluated mRNA levels of key fibrosis-related genes, collagen 1a1

and α-SMA, in the liver of ARB-treated BDL rats by real time RT-PCR. Collagen 1a1 and α-SMA mRNA levels were increased in the BDL group by 3.7 and 3.8-fold compared with the Sham group, respectively, and ARB treatment reduced the expression of them by 44% and 52%, respectively (**Figure 21**; page 98). These results are consistent with the histological results in that collagen deposition, α-SMA-positive cells and hydroxyproline content were reduced.

TGF-β1 is a key pro-fibrogenic cytokine and is thought to stimulate activation of HSCs, in particular collagen production in HSCs. Therefore, I evaluated plasma TGF-β1 levels in ARB-treated BDL rats. Plasma TGF-β1 levels were increased in the BDL group by 1.7-fold compared with the Sham group, and ARB treatment reduced them by 79% (**Figure 22**; page 99). These results indicate that Ang II is involved in plasma TGF-β1 elevation *in vivo*.

Effects of Ang II on liver injury in BDL rats *in vivo*

In order to evaluate the effects of Ang II on liver injury, plasma markers of liver injury were measured. Plasma AST and ALT levels were increased in the BDL group by 5.3 and 2.6-fold compared with the Sham group, respectively (**Figure 23**; page 100). However, ARB treatment did not significantly change plasma AST and ALT levels. These results indicate that ARB did not directly ameliorate liver injury in BDL rats. Therefore, the anti-fibrotic effects of ARB were not secondary ones due to hepatoprotection.

Effects of Ang II on proliferation and collagen synthesis in activated HSCs *in vitro*

In the *in vivo* experiments, possible fibrogenic effects of Ang II were shown. Next, in order to investigate the mechanism of fibrogenic action of Ang II, I evaluated the effects of Ang II on activated HSCs *in vitro*. HSCs were prepared from rats by collagenase-pronase perfusion and cultured. Isolated HSCs show a quiescent phenotype with a round shape and stored vitamin A within the cells. Cultured HSCs on plastic dishes were spontaneously activated during several days and thereafter used for experiments. Olmesartan is a prodrug that converts to an active metabolite in blood. Therefore, a pharmacologically active form of olmesartan,

RNH-6270 was used in the *in vitro* experiments.

First, I evaluated the effects of Ang II on proliferation and collagen synthesis as typical and crucial phenotypes of activated HSCs. Ang II treatment stimulated proliferation of activated HSCs, measured as [^{3}H]thymidine incorporation into cells (**Figure 24**; page 101). ARB treatment completely blocked the Ang II-stimulated proliferation in activated HSCs. Ang II treatment also stimulated collagen synthesis in activated HSCs, measured as [^{3}H]proline incorporation (**Figure 25**; page 102). ARB treatment almost completely blocked the Ang II-induced collagen synthesis in activated HSCs. These results demonstrate that Ang II stimulates typical fibrogenic phenotypes including proliferation and collagen synthesis in activated HSCs through activation of AT1 receptors.

Effects of Ang II on autocrine production of pro-fibrogenic cytokines in activated HSCs *in vitro*

TGF-β1 plays a central role in transformation of HSCs to myofibroblast-like phenotypes in a paracrine manner. Furthermore, activated HSCs secrete TGF-β1 and stimulate self-activation in an autocrine manner. Therefore, I evaluated the effects of Ang II on production of TGF-β1 in activated HSCs. Ang II increased TGF-β1 levels in culture supernatants in a dose-dependent manner (**Figure 26-A**; pages 103 and 104). PDGF is the most potent mitogen for HSCs; therefore I evaluated TGF-β1 production after PDGF treatment. PDGF increased TGF-β1 production in activated HSCs in my present study. Interestingly, Ang II and PDGF additively stimulated TGF-β1 production in activated HSCs. ARB treatment almost completely blocked the Ang II-induced TGF-β1 production in activated HSCs (**Figure 26-B**; pages 103 and 104).

In addition to TGF-β1, CTGF is also a key pro-fibrogenic cytokine in activated HSCs. Therefore, I evaluated the effects of Ang II on mRNA expression of CTGF in activated HSCs. Ang II treatment significantly increased mRNA expression of CTGF in activated HSCs (**Figure 27**; page 105). ARB treatment completely blocked Ang II-induced CTGF mRNA expression. These results suggest that up-regulation of TGF-β1 and CTGF possibly mediates fibrogenic

action of Ang II in activated HSCs.

Discussion

In this chapter, I demonstrated that Ang II plays a key role in the progression of liver fibrosis mediated through stimulation of proliferation and collagen synthesis of activated HSCs. I showed that ARB, olmesartan ameliorated liver fibrosis in BDL rats. During the same period as my research, two other groups had also reported anti-fibrotic effects of ARB in liver *in vivo* (Paizis et al., 2001; Yoshiji et al., 2001). Paizis et al. used BDL models to evaluate ARB, irbesartan just like my study. They showed that ARB reduced mRNA levels of collagen 1a1 in the liver; however they failed to show decrease of collagen protein levels or amelioration of liver histology. In contrast, I showed that olmesartan surely attenuated liver fibrosis histologically and decreased collagen protein levels as well as mRNA levels of collagen 1a1 of BDL rats. Yoshiji et al. also reported that ARB, candesartan, inhibited progression of liver fibrosis in pig-serum models. My results and their findings indicate key roles of Ang II in liver fibrosis through activation of AT1 receptors. In my present study, ARB did not significantly affect plasma markers of liver injury, AST and ALT, although ARB ameliorated liver fibrosis. These results exclude the possibility of indirect effects of ARB on liver fibrosis mediated through hepatocellular protection.

In order to elucidate the mechanism of fibrogenic action of Ang II, I evaluated the effects of Ang II and ARB on typical phenotypes of activated HSCs *in vitro*. Quiescent HSCs in normal livers are not or scarcely proliferating; however activated HSCs in injured livers are highly proliferating. Batallar et al. reported that Ang II stimulated proliferation of human HSCs (Bataller et al., 2000). I also demonstrated that Ang II treatment stimulated proliferation of activated HSCs *in vitro*, measured as [^{3}H]thymidine incorporation into cells, and ARB treatment completely blocked them. In an injured liver, activated HSCs continuously produce collagen and other ECM that lead to development of liver fibrosis. Ang II treatment also stimulated collagen synthesis measured as [^{3}H]proline incorporation, and ARB treatment blocked them. I showed for the first

time that Ang II stimulated collagen production, which is the most crucial phenotype of activated HSCs.

TGF-β1 is highly involved in the pathogenesis of liver fibrosis. TGF-β1 mainly stimulates the activation and collagen synthesis of HSCs in an autocrine or a paracrine manner (Matsuoka and Tsukamoto, 1990; Gressner, 1995). In BDL model, TGF-β1 expression was up-regulated in the liver and HSCs were shown to be their main source of production (Bissell et al., 1995). In other organs such as the kidney and heart, the expression of TGF-β1 was increased with stimulation of Ang II (Weber, 1997). Furthermore, Yoshiji et al. showed that ARB treatment decreased protein levels of TGF-β1 in the liver of fibrotic rats (Yoshiji et al., 2001). I also showed that plasma levels of TGF-β1 were increased in BDL rats *in vivo* and ARB treatment attenuated them. Additionally, I showed that Ang II treatment increased TGF-β1 production of activated HSCs *in vitro*. PDGF is the most potent mitogen for HSCs (Pinzani, 2002; Borkham-Kamphorst et al., 2007). PDGF also induced TGF-β1 production in activated HSCs in my present study. Interestingly, PDGF treatment potentiated the Ang II-induced TGF-β1 production. These results suggest that Ang II and PDGF may jointly stimulate activated phenotypes including TGF-β1 production in HSCs and lead to development of liver fibrosis. ARB treatment almost completely blocked the Ang II-induced TGF-β1 production in activated HSCs *in vitro* and additionally inhibited increased plasma TGF-β1 levels in BDL rats *in vivo*. CTGF is also thought to stimulate activation of HSCs (Paradis et al., 1999; Williams et al., 2000; Paradis et al., 2002). My results indicated for the first time that Ang II treatment up-regulates mRNA expression of CTGF in activated HSCs. These results suggest that the Ang II-stimulated collagen synthesis is mediated through up-regulation of two pro-fibrogenic cytokines, TGF-β1 and CTGF, to some extent in an autocrine manner. All of these actions were mediated through activation of AT1 receptors because all of them were blocked with ARB treatment.

Histological analyses showed remarkable collagen deposition in the liver of BDL rats. The α-SMA-positive cells, indicative of activated HSCs, were accumulated in the area of collagen deposition. The mRNA levels of α-SMA were also up-regulated in the liver of BDL rats. These results support that proliferating

and activated HSCs are involved in development of fibrosis in the liver of BDL rats. ARB treatment decreased accumulation of α-SMA-positive cells and mRNA expression of α-SMA as well as collagen deposition, suggesting that Ang II and AT1 receptors contribute to the activation and proliferation of HSCs in the liver of BDL rats. As expected, α-SMA-positive cells seemed to express AT1 receptors based on the AT1 immunostaining. Paizis et al. also reported remarkable expression of AT1 receptors and other RAS components in the fibrotic area in the liver of BDL rats (Paizis et al., 2002). Furthermore, activated, but not quiescent, HSCs highly expressed RAS components and synthesized Ang II (Bataller et al., 2003b). Therefore, activation of local RAS in the liver after liver injury may play a key role in liver fibrosis in chronic liver diseases including NASH. My data and these other reports demonstrated that activated HSCs expressing AT1 receptors, in response to Ang II, play a key role in the progression of liver fibrosis. Particularly, I showed that Ang II stimulated collagen synthesis of activated HSCs is possibly mediated through up-regulation of pro-fibrogenic cytokines including TGF-β1 and CTGF. AT2 receptors generally have divergent pathways compared with AT1 receptors. Interestingly, it has been predicted that ARB increases levels of unbound Ang II after AT1 receptor blockade and subsequently activates AT2 receptors (Unger, 2002). Therefore, activation of AT2 receptors as well as AT1 receptor blockade may also contribute to the beneficial effects of ARB. Nabeshima et al. reported that liver fibrosis is deteriorated in AT2 receptor-deficient mice (Nabeshima et al., 2006). I suppose that AT2 receptor activation also in some content contributed to anti-fibrotic effects of ARB in addition to AT1 receptor blockade in my present study.

As discussed above, some researchers and I concurrently elucidated the fibrogenic effects and the molecular mechanism of Ang II in chronic liver disease. After our results were published, some new findings about roles of Ang II in NASH/NAFLD or liver fibrosis have been reported as following, 1) contribution of reactive oxygen species to Ang II-induced liver fibrosis, 2) roles of RAS in the development of hepatic steatosis in NASH/NAFLD and 3) clinical trials of ARBs in liver fibrosis including NASH/NAFLD patients.

Increased oxidative stress is thought to lead to activation of HSCs and

liver fibrosis (Koek et al., 2011). Systemic infusion of Ang II to normal or fibrotic rats induced activation of HSCs and consequently liver fibrosis mediated through increased oxidative stress and pro-inflammatory cytokines (Bataller et al., 2003a, 2005). Ang II phophorylated $p47^{phox}$, a subunit of NADPH oxidase, and induced reactive oxygen species via NADPH oxidase activity in human HSCs (Bataller et al., 2003c). Ang II-induced activation of HSCs was also attenuated by treatment of NADPH oxidase inhibitors and HSCs isolated from $p47^{phox}$-deficient mice showed blunted responses to Ang II. Furthermore, $p47^{phox}$-deficiency attenuated liver fibrosis after BDL. Therefore, NADPH oxidase-mediated oxidative stress is thought to contribute to Ang II-induced activation of HSCs and development of liver fibrosis.

In summary, AT1 receptor blockade reduced activated HSCs and prevented progression of liver fibrosis *in vivo*, and Ang II stimulated proliferation and collagen synthesis in activated HSCs *in vitro* possibly through increased production of TGF-β1 and CTGF (summarized in **Figure 28**; page 106). These results demonstrate that Ang II plays an important role in the progression of liver fibrosis in NASH.

General Discussion

Since the publication of my research, the involvement of RAS including Ang II in metabolic disorders has been reported (Putnam et al., 2012). Liver-specific disruption of AT1 receptors or ARBs have been shown to attenuate triglyceride accumulation in the liver and in turn inflammation and fibrosis in NASH models including MCD models, indicating contribution of Ang II to hepatic steatosis in NASH/NAFLD concerned with insulin resistance (Fujita et al., 2007; Hirose et al., 2007; Kurita et al., 2008; Nabeshima et al., 2009). Therefore, the mechanism of beneficial effects of AT1 receptor blockade in NASH models is complicated. Some mechanisms in Ang II-induced triglyceride accumulation in the liver have been proposed including decreased fatty acid oxidation, increased VLDL secretion and increased *de novo* lipogenesis (Ran et al., 2004a, 2004b; Kurita et al., 2008; Rong et al., 2010). On the other hand, SCD-1 potently contributes to process of lipogenesis and triglyceride synthesis in the liver. Interestingly, Yokozawa et al. reported that ARB down-regulates liver SCD-1 expression and ameliorates insulin resistance and hepatic steatosis in obese rats (Yokozawa et al., 2009). These findings suggest that, in addition to liver fibrosis, Ang II also plays a key role in hepatic steatosis, and these effects are possibly mediated through SCD-1 regulation to some extent. Therefore, Ang II may modulate NASH pathology in multiple processes.

In my present study, the SCD-1 inhibitor and ARB were used as tool compounds to evaluate the roles of SCD-1 and Ang II, respectively. These proteins are attractive targets to treat NASH/NAFLD; therefore both compounds may be useful to treat NASH/NAFLD. I showed that SCD-1 is related to the early phases of NASH. SCD-1 inhibitors may be useful to prevent the onset of NASH in patients with simple steatosis or progression of NASH in patients with early phases of NASH. In contrast, steatosis, in which SCD-1 activity mainly involved, is a trigger to steatohepatitis but the roles in acceleration of disease after the onset of NASH are unknown. Therefore, I suppose that the benefit of SCD-1 inhibitors are restrictive at advanced stages of patients. In order to confirm the potential of SCD-1 inhibitor in advanced stages of patients, it is important to evaluate therapeutic protocol in which treatment of the SCD-1 inhibitor is started after establishment of the disease in MCD models. Additionally, SCD-1 deficiency

developed cutaneous abnormalities and narrow eye fissure with atrophic sebaceous and meibomian glands due to defect of lipid synthesis in tissues (Miyazaki et al., 2001b). SCD-1 also seems to be associated with inflammation in some organs (Liu et al., 2011). SCD-1 inhibitor did not cause inflammatory observation; however other compounds with more potent systemic inhibition of SCD-1 increased white blood cell (Uto et al., 2011). Therefore, liver-specific inhibition may be important to avoid these adverse effects.

My studies as well as other groups showed beneficial effects of ARBs in animal models with chronic liver disease. Furthermore, as discussed above, Ang II possibly contributes to hepatic steatosis and other metabolic disorders in addition to liver fibrosis. Therefore, ARBs might be useful to treat patients with broad stages in NASH/NAFLD such as early steatotic or advanced fibrotic stages. Since the publication of our findings, some clinical trials of ARBs in treatment of liver fibrosis including NASH patients have been reported (Yokohama et al., 2004, 2006; Georgescu et al., 2009; Fogari et al., 2012). These studies showed possible beneficial effects of ARBs on inflammation, liver injury and metabolic disorders in NASH patients. However, they were all small size scale and clinical endpoints (histology, serum markes, etc.) and the study designs (duration of treatment, severity of patients, etc.) were quite different among studies. Furthermore, only few trials showed a reduction of fibrosis, the most important pathology of NASH, in histological evaluation with liver biopsy. I think that in order to fully elucidate the benefit of ARBs in NASH patients, large scale and placebo-controlled trials with long-term histological evaluation are needed. ARBs are highly safe and widely treated in the world. If the benefits of ARBs are established in large scale clinical trials, these will provide promising treatment of NASH/NAFLD.

In conclusion, I demonstrated that SCD-1 plays an important role in the onset phase of NASH, and Ang II in the progression of liver fibrosis (summarized in **Figure 29**; page 117).

Acknowledgements

I am deeply grateful to Prof. Tomoki Chiba (Univ. of Tsukuba) for his guidance and encouragement throughout the course of my research and doctoral thesis.

I would like to express my gratitude to Prof. Hideko Urushihara (Univ. of Tsukuba), Prof. Kouji Nakamura (Univ. of Tsukuba) and Assoc. Prof. Kazuichi Sakamoto (Univ. of Tsukuba) for helpful advice and comments to my research and thesis.

I would like to express my gratitude to Dr. Ryuta Koishi (Daiichi Sankyo Co., Ltd), Dr. Takashi Fukuoka (DS) and Dr. Fujio Isono (DS) for tremendous support and encouragement for my study in doctoral course.

I also wish to thank Dr. Toshiyuki Takagi (DS), Ms. Satoko Wakimoto (DS), Dr. Yoshikazu Uto (DS), Mr. Hideki Terashima (DS), Dr. Keita Kono (DS), Dr. Tsuneaki Ogata (DS), Dr. Jun Ohsumi (DS), Ms. Miwa Suga, Ms. Shoko Honzumi (DS), Mr. Keisuke Yamada (DS) and Mr. Hirokazu Ishikawa (Daiichi Sankyo RD Novare Co., Ltd) for significant contribution in my research, helpful advice and discussion, Ms. Yuko Ueno (DS) and Dr. Yohei Kiyotsuka (DS) for synthesizing and providing compound A, Dr. Tomohiro Nishizawa (DS), Ms. Nobumi Nagaoka (DS), Ms. Yuka Morikawa (DS), Dr. Fumihiko Matsuda (DS), Dr. Atsuhiro Sugidachi (DS) for enormous help and support in my research, and Mr. Haruki Domon (DS), Ms. Noriko Kobayashi (DS), Dr. Katsuhiko Nawa (DS), Ms. Yuko Ozawa (DS) and all members of Venture Science Laboratories in Daiichi Sankyo Co., Ltd for various support during my doctoral course.

I would like to express the deepest appreciation to Daiichi Sankyo Co., Ltd for financial support.

Finally, I also want to thank all my friends, co-workers and family.

References

Bataller R, Ginès P, Nicolás JM, Görbig MN, Garcia-Ramallo E, Gasull X, Bosch J, Arroyo V, Rodés J (2000). Angiotensin II induces contraction and proliferation of human hepatic stellate cells. *Gastroenterology*, **118**, 1149-1156.

Bataller R, Gabele E, Schoonhoven R, Morris T, Lehnert M, Yang L, Brenner DA, Rippe RA (2003a). Prolonged infusion of angiotensin II into normal rats induces stellate cell activation and proinflammatory events in liver. *Am J Physiol Gastrointest Liver Physiol*, **285**, G642–G651.

Bataller R, Sancho-Bru P, Ginès P, Lora JM, Al-Garawi A, Solé M, Colmenero J, Nicolás JM, Jiménez W, Weich N, Gutiérrez-Ramos JC, Arroyo V, Rodés J (2003b). Activated human hepatic stellate cells express the renin-angiotensin system and synthesize angiotensin II. *Gastroenterology*, **125**, 117–125.

Bataller R, Schwabe RF, Choi YH, Yang L, Paik YH, Lindquist J, Qian T, Schoonhoven R, Hagedorn CH, Lemasters JJ, Brenner DA. (2003c). NADPH oxidase signal transduces angiotensin II in hepatic stellate cells and is critical in hepatic fibrosis. *J Clin Invest*, **112**, 1383–1394.

Bataller R, Gabele E, Parsons CJ, Morris T, Yang L, Schoonhoven R, Brenner DA, Rippe RA (2005). Systemic infusion of angiotensin II exacerbates liver fibrosis in bile duct-ligated rats. *Hepatology*, **41**, 1046–1055.

Belfort R, Harrison SA, Brown K, Darland C, Finch J, Hardies J, Balas B, Gastaldelli A, Tio F, Pulcini J, Berria R, Ma JZ, Dwivedi S, Havranek R, Fincke C, DeFronzo R, Bannayan GA, Schenker S, Cusi K (2006). A placebo controlled trial of pioglitazone in subjects with nonalcoholic steatohepatitis. *N Eng J Med*, **355**, 15–25.

Bissell DM, Wang SS, Jarnagin WR, Roll FJ (1995). Cell-specific expression of transforming growth factor-beta in rat liver. Evidence for autocrine regulation of hepatocyte proliferation. *J Clin Invest*, **96**, 447-455.

Borkham-Kamphorst E, van Roeyen CR, Ostendorf T, Floege J, Gressner AM, Weiskirchen R (2007). Pro-fibrogenic potential of PDGF-D in liver fibrosis. *J Hepatol*, **46**, 1064-74.

Brewster UC, Setaro JF, Perazella MA (2003). The renin–angiotensin–aldosterone system: cardiorenal effects and implications for renal and cardiovascular disease states. *Am J Med Sci*, **326**, 15–24.

Brilla CG (2000). Renin-angiotensin-aldosterone system and myocardial fibrosis. *Cardiovasc Res*, **47**, 1-3.

Buqué X, Martínez MJ, Cano A, Miquilena-Colina ME, García-Monzón C, Aspichueta P, Ochoa B (2010). A subset of dysregulated metabolic and survival genes is associated with severity of hepatic steatosis in obese Zucker rats. *J Lipid Res*, **51**, 500-513.

Chen G, Liang G, Ou J, Goldstein JL, Brown MS (2004). Central role for liver X receptor in insulin-mediated activation of Srebp-1c transcription and stimulation of fatty acid synthesis in liver. *PNAS*, **101**, 11245-11250.

Czaja MJ, Geerts A, Xu J, Schmiedeberg P, Ju Y (1994). Monocyte chemoattractant protein 1 (MCP-1) expression occurs in toxic rat liver injury and human liver disease. *J Leukoc Biol*, **55**, 120-126.

Day CP, James OF (1998). Steatohepatitis: A tale of two "hits"? *Gastroenterology*, **114**, 842-845.

Donnelly KL, Smith CI, Scwarzenberg SJ, Jessurun J, Boldt MD, Parks EJ (2005). Sources of fatty acids stored in liver and secreted via lipoproteins in patients with nonalcoholic fatty liver disease. *J Clin Invest*, **115**, 1343-1351.

Eitel K, Staiger H, Brendel MD, Brandhorst D, Bretzel RG, Haring HU, Kellerer M (2002). Different role of saturated and unsaturated fatty acids in beta-cell apoptosis. *Biochem Biophys Res Commun*, **299**, 853–856.

Fan JG, Qiao L (2009). Commonly used animal models of non-alcoholic steatohepatitis. *Hepatobilliary Pancreat Dis Int*, **8**, 233-240.

Farrell GC, Larter CZ (2006). Nonalcoholic fatty liver disease: from steatosis to cirrhosis. *Hepatology*, **43**, S99-S112.

Festi D, Schiumerini R, Marzi L, Di Biase AR, Mandolesi D, Montrone L, Scaioli E, Bonato G, Marchesini-Reggiani G, Colecchia A (2013). Review article: the diagnosis of non-alcoholic fatty liver disease – availability and accuracy of non-invasive methods. *Aliment Pharmacol Ther*, **37**, 392–400.

Flowers MT, Groen AK, Oler AT, Keller MP, Choi Y, Schueler KL, Richards OC, Lan H, Miyazaki M, Kuipers F, Kendziorski CM, Ntambi JM, Attie AD (2006). Cholestasis and hypercholesterolemia in SCD1-deficient mice fed a low-fat, high-carbohydrate diet. *J Lipid Res*, **47**, 2668-80.

Flowers MT, Keller MP, Choi Y, Lan H, Kendziorski C, Ntambi JM, Attie AD (2008). Liver gene expression analysis reveals endoplasmic reticulum stress and metabolic dysfunction in SCD1-deficient mice fed a very low-fat diet. *Physiol Genomics*, **33**, 361-72.

Flowers MT, Ade L, Strable MS, Ntambi JM (2012). Combined deletion of SCD1 from adipose tissue and liver does not protect mice from obesity. *J Lipid Res*, **53**, 1646-53.

Fogari R, Maffioli P, Mugellini A, Zoppi A, Lazzari P, Derosa G (2012). Effects of losartan and amlodipine alone or combined with simvastatin in hypertensive patients with nonalcoholic hepatic steatosis. *Eur J Gastroenterol Hepatol*, **24**, 164–171.

Friedman SL (2008). Hepatic stellate cells: protean, multifunctional, and enigmatic cells of the liver. *Physiol Rev*, **88**, 125–172.

Fujita K, Yoneda M, Wada K, Mawatari H, Takahashi H, Kirikoshi H, Inamori M, Nozaki Y, Maeyama S, Saito S, Iwasaki T, Terauchi Y, Nakajima A (2007). Telmisartan, an angiotensin II type 1 receptor blocker, controls progress of nonalcoholic steatohepatitis in rats. *Dig Dis Sci*, **52**, 3455–3464.

George J, Roulot D, Koteliansky VE, Bissell DM (1999). *In vivo* inhibition of rat stellate cell activation by soluble transforming growth factor β type II receptor: a potential new therapy for hepatic fibrosis. *PNAS*, **96**, 12719-12724.

Georgescu EF, Ionescu R, Niculescu M, Mogoanta L, Vancica L (2009). Angiotensin-receptor blockers as therapy for mild-to-moderate hypertension associated non-alcoholic steatohepatitis. *World J Gastroenterol*, **15**, 942–954.

Gomez-Dominguez E, Gisbert JP, Moreno-Monteagudo JA, Garcia-Buey L, Moreno-Otero R (2006). A pilot study of atorvastatin in dyslipidemic, non-alcoholic fatty liver patients. *Aliment Pharmacol Ther*, **23**, 1643-1647.

Greco D, Kotronen A, Westerbacka J, Puig O, Arkkila P, Kiviluoto T, Laitinen S, Kolak M, Fisher RM, Hamsten A, Auvinen P, Yki-Järvinen H (2008). Gene expression in human NAFLD. *Am J Physiol Gastroenterol Liver Physiol*, **294**, G1281-1287.

Gressner AM (1995). Cytokines and cellular crosstalk involved in the activation of fat-storing cells. *J Hepatol*, **22 Suppl**, 28-36.

Harrison SA, Ramrakhiani S, Brunt EM, Anabari MA, Cortese C, Bacon BR (2003a). Orlistat in the treatment of NASH: a case series. *Am J Gasteroenterol*, **98**, 926-930.

Harrison SA, Torgerson S, Hayashi P, Ward J, Schenker S (2003b). Vitamin E and C treatment improves fibrosis in patients with nonalcoholic steatohepatitis. *Am J Gastroenterol*, **98**, 2485–2490.

Hernandez-Gea V, Friedman SL (2011). Pathogenesis of liver fibrosis. *Annu Rev Pathol Mech Dis*, **6**, 425-456.

Hirose A, Ono M, Saibara T, Nozaki Y, Masuda K, Yoshioka A, Takahashi M, Akisawa N, Iwasaki S, Oben JA, Onishi S (2007). Angiotensin II type 1 receptor blocker inhibits fibrosis in rat nonalcoholic steatohepatitis. *Hepatology*, **45**, 1375–1381.

Ishidoya S, Morrissey J, McCracken R, Reyes A, Klahr S (1995). Angiotensin II receptor antagonist ameliorates renal tubulointerstitial fibrosis caused by unilateral ureteral obstruction. *Kidney Int*, **47**, 1285-1294.

Issandou M, Bouilot A, Brusq JM, Forest MC, Grillot D, Guillard R, Martin S, Michiels C, Sulpice T, Daugan A (2009). Pharmacological inhibition of stearoyl-CoA desaturase 1 improves insulin sensitivity in insulin-resistant rat models. *Eur J Pharmacol*, **618**, 28-36.

Jonsson JR, Clouston AD, Ando Y, Kelemen LI, Horn MJ, Adamson MD, Purdie DM, Powell EE (2001). Angiotensin-converting enzyme inhibition attenuates the progression of rat hepatic fibrosis. *Gastroenterology*, **121**, 148-155.

Kagami S, Border WA, Miller DE, Noble NA (1994). Angiotensin II stimulates extracellular matrix protein synthesis through induction of transforming growth factor-beta expression in rat glomerular mesangial cells. *J Clin Invest*, **93**, 2431-2437.

Kawada N, Seki S, Inoue M, Kuroki T (1998). Effect of antioxidants, resveratrol, quercetin, and N-acetylcysteine, on the functions of cultured rat hepatic stellate cells and Kupffer cells. *Hepatology*, **27**, 1265-1274.

Kim S, Ohta K, Hamaguchi A, Omura T, Yukimura T, Miura K, Inada Y, Ishimura Y, Chatani F, Iwao H (1995). Angiotensin II type 1 receptor antagonist inhibits the gene expression of transforming growth factor-β1 and extracellular matrix in cardiac and vascular tissues of hypertensive rats. *J Pharmacol Exp Ther*, **273**, 509-515.

Koek GH, Liedorp PR, Bast A (2011). The role of oxidative stress in non-alcoholic steatohepatitis. *Clin Chim Acta*, **412**, 1297-305.

Koltun DO, Vasilevich NI, Parkhill EQ, Glushkov AI, Zilbershtein TM, Mayboroda EI, Boze MA, Cole AG, Henderson I, Zautke NA, Brunn SA, Chu N, Hao J, Mollova N, Leung K, Chisholm JW, Zablocki J (2009). Orally bioavailable, liver-selective stearoyl-CoA desaturase (SCD) inhibitors. *Bioorg Med Chem Lett*, **19**, 3050-3.

Kotronen A, Seppanen-Laakso T, Westerbacka J, Kiviluoto T, Arola J, Ruskeepaa AL, Oresic M, Yki-Jarvinen H (2009). Hepatic stearoyl-CoA desaturase (SCD)-1 activity and diacylglycerol but not ceramide concentrations are increased in the nonalcoholic human fatty liver. *Diabetes*, **58**, 203-208.

Kountouras J, Billing BH, Scheuer PJ (1984). Prolonged bile duct obstruction: a new experimental model for cirrhosis in the rat. *Br J Exp Path*, **65**, 305-311.

Kurita S, Takamura T, Ota T, Matsuzawa-Nagata N, Kita Y, Uno M, Nabemoto S, Ishikura K, Misu H, Ando H, Zen Y, Nakanuma Y, Kaneko S (2008). Olmesartan ameliorates a dietary rat model of non-alcoholic steatohepatitis through its pleiotropic effects. *Eur J Pharmacol*, **588**, 316–324.

Larter CZ, Yeh MM, Haigh WG, Williams J, Brown S, Bell-Anderson KS, Lee SP, Farrell GC (2008). Hepatic free fatty acids accumulate in experimental steatohepatitis: role of adaptive pathways. *J Hepatol*, **48**, 638-647.

Leask A, Holmes A, Abraham DJ (2002). Connective tissue growth factor: a new and important player in the pathogenesis of fibrosis. *Curr. Pheumatol Rep*, **4**, 136-142.

Lewis GF, Carpentier A, Adeli K, Giacca A (2002). Disordered fat storage and mobilization in the pathogenesis of insulin resistance and type 2 diabetes. *Endocr Rev*, **23**, 201-229.

Li Z, Berk M, Mclntyre TM, Feldstein AE (2009). Hepatic lipid partitioning and liver damage in nonalcoholic fatty liver disease: role of stearoyl-CoA desaturase. *J Biol Chem*, **284**, 5637-5644.

Liu X, Strable MS, Ntambi JM (2011). Stearoyl CoA desaturase 1: role in cellular inflammation and stress. *Adv Nutr*, **2**, 15-22.

Malhi H, Barreyro FJ, Isomoto H, Bronk SF, Gores GJ (2007). Free fatty acids sensitize hepatocytes to TRAIL mediated cytotoxicity. *Gut*, **56**, 1124-1131.

Malinowski SS, Byrd JS, Bell AM, Wofford MR, Riche DM (2013). Pharmacologic therapy for nonalcoholic fatty liver disease in adults. *Pharmacotherapy*, **33**, 223–242.

Marchesini G, Brizi M, Bianchi G, Tomassetti S, Zoli M, Melchionda N (2001). Metformin in non-alcoholic steatohepatitis. *Lancet*, **358**, 893-894.

Marra F, Valente AJ, Pinzani M, Abboud HE (1993). Cultured human liver fat storing cells produce monocyte chemotactic protein-1: regulation by proinflammatory cytokines. *J Clin Invest*, **92**, 1674-1680.

Marra F, Romanelli RG, Giannini C, Failli P, Pastacaldi S, Arrighi MC, Pinzani M, Laffi G, Montalto P, Gentilini P (1999). Monocyte chemotactic protein-1 as a chemoattractant for human hepatic stellate cells. *Hepatology*, **29**, 140-148.

Matsuoka M, Tsukamoto H (1990). Stimulation of hepatic lipocyte collagen production by Kuppfer cell-derived transforming growth factor β: implications for a pathogenetic role in alcoholic liver fibrogenesis. *Hepatology*, **11**, 599-605.

Matsuzawa N, Takamura T, Kurita S, Misu H, Ota T, Ando H, Yokoyama M, Honda M, Zen Y, Nakanuma Y, Miyamoto K, Kaneko S (2007). Lipid-induced oxidative stress causes steatohepatitis in mice fed an atherogenic diet. *Hepatology*, **46**, 1392-1403.

Mehta PK, Griendling KK (2007). Angiotensin II cell signaling: physiological and pathological effects in the cardiovascular system. *Am J Physiol Cell Physiol*, **292**, C82–C97.

Miyazaki M, Kim YC, Gray-Keller MP, Attie AD, Ntambi JM (2000). The biosynthesis of hepatic cholesterol esters and triglycerides is impaired in mice with a disruption of the gene for stearoyl-CoA desaturase 1. *J Biol Chem*, **275**, 30132-30138.

Miyazaki M, Kim YC, Ntambi JM (2001a). A lipogenic diet in mice with a disruption of the stearoyl-CoA desaturase 1 gene reveals a stringent requirement of endogenous monounsaturated fatty acids for triglyceride synthesis. *J Lipid Res*, **42**, 1018-1024.

Miyazaki M, Man WC, Ntambi JM (2001b). Targeted disruption of stearoyl-CoA desaturase1 gene in mice causes atrophy of sebaceous and meibomian glands and depletion of wax esters in the eyelid. *J Nutr*, **131**, 2260–8.

Miyazaki M, Dobrzyn A, Man WC, Chu K, Sampath H, Kim HJ, Ntambi JM (2004). Stearoyl-CoA desaturase 1 gene expression is necessary for fructose-mediated induction of lipogenic gene expression by sterol regulatory element-binding protein-1c-dependent and –independent mechanisms. *J Biol Chem*, **279**, 25164-25171.

Miyazaki M, Flowers MT, Sampath H, Chu K, Otzelberger C, Liu X, Ntambi JM (2007). Hepatic stearoyl-CoA desaturase-1 deficiency protects mice from carbohydrate-induced adiposity and hepatic steatosis. *Cell Metab*, **6**, 484-496.

Mizuno M, Sada T, Ikeda M, Fukuda N, Miyamoto M, Yanagisawa H, Koike H (1995). Pharmacology of CS-866, a novel nonpeptide angiotensin II receptor antagonist. *Eur J Pharmacol*, **285**, 181-188.

Molteni A, Moulder JE, Cohen EF, Ward WF, Fish BL, Taylor JM, Wolfe LF, Brizio-Molteni L, Veno P (2000). Control of radiation-induced pneumopathy and lung fibrosis by angiotensin-converting enzyme inhibitors and an angiotensin II type 1 receptor blocker. *Int J Radiat Biol*, **76**, 523-532.

Nabeshima Y, Tazuma S, Kanno K, Hyogo H, Iwai M, Horiuchi M, Chayama K (2006). Anti-fibrogenic function of angiotensin II type 2 receptor in CCl4-induced liver fibrosis. *Biochem Biophys Res Commun*. **346**, 658–664.

Nabeshima Y, Tazuma S, Kanno K, Hyogo H, Chayama K (2009). Deletion of angiotensin II type I receptor reduces hepatic steatosis. *J Hepatol*, **50**, 1226–1235.

Ntambi JM (1995). The regulation of stearoyl-CoA desaturase (SCD). *Prog Lipid Res*, **34**, 139-150.

Ntambi JM, Miyazaki M, Stoehr JP, Lan H, Kendziorski CM, Yandell BS, Song Y, Cohen P, Friedman JM, Attie AD (2002). Loss of stearoyl-CoA desaturase-1 function protects mice against adiposity. *PNAS*, **99**, 11482-11486.

Ohishi T, Saito H, Tsusaka K, Toda K, Inagaki H, Hamada Y, Kumagai N, Atsukawa K, Ishii H (2001). Anti-fibrogenic effect of an angiotensin converting enzyme inhibitor on chronic carbon tetrachloride-induced hepatic fibrosis in rats. *Hepatol Res*, **21**, 147-158.

Paizis G, Gilbert RE, Cooper ME, Murthi P, Schembri JM, Wu LL, Rumble JR, Kelly DJ, Tikellis C, Cox A, Smallwood RA, Angus PW (2001). Effect of angiotensin II type 1 receptor blockade on experimental hepatic fibrogenesis. *J Hepatol*, **35**, 376-385.

Paizis G, Cooper ME, Schembri JM, Tikellis C, Burrell LM, Angus PW (2002). Up-regulation of components of the rennin-angiotensin system in the bile duct-ligated rat liver. *Gastroenterology*, **123**, 1667-1676.

Paradis V, Dargere D, Vidaud M, De Gouville AC, Huet S, Martinez V, Gauthier JM, Ba N, Sobesky R, Ratziu V, Bedossa P (1999). Expression of connective tissue growth factor in experimental rat and human liver fibrosis. *Hepatology*, **30**, 968-976.

Paradis V, Dargere D, Bonvoust F, Vidaud M, Segarini P, Bedossa P (2002). Effects and regulation of connective tissue growth factor on hepatic stellate cells. *Lab Invest*, **82**, 767-773.

Paul M, Royan MA, Kreutz R (2006). Physiology of local renin-angiotensin systems. *Physiol Rev*, **86**, 747-803.

Peter S (2011). Animal models for the study of hepatic fibrosis. *Best Prac Res Clin Gastroenterol*, **25**, 319-333.

Pinzani M (2002). PDGF and signal transduction in hepatic stellate cells. *Front Biosci*, **7**, d1720-6.

Puri P, Baillie RA, Wiest MM, Mirshahi F, Choudhery J, Cheung O, Sargeant C, Contos MJ, Sanyal AJ (2007). A lipidomic analysis of nonalcoholic fatty liver disease. *Hepatology*, **46**, 1081-1090.

Putnam K, Shoemaker R, Yiannikouris Y, Cassis LA (2012). The renin-angiotensin system: a target of and contributor to dyslipidemias, altered glucose homeostasis, and hypertension of the metabolic syndrome. *Am J Physiol Heart Circ Physiol*, **302**, H1219-30.

Qi Z, Atsuchi N, Ooshima A, Takeshita A, Ueno H (1999). Blockade of type β transforming growth factor signaling prevents liver fibrosis and dysfunction in the rat. *PNAS*, **96**, 2345-2349.

Rahman SM, Dobrzyn A, Dobrzyn P, Lee SH, Miyazaki M, Ntambi JM (2003). Stearoyl-CoA desaturase 1 deficiency elevates insulin-signaling components and down-regulates protein-tyrosine phosphatase 1B in muscle. *PNAS*, **100**, 11110-11115.

Rahman SM, Dobrzyn A, Lee SH, Dobrzyn P, Miyazaki M, Ntambi JM (2005). Stearoyl-CoA desaturase 1 deficiency increases insulin signaling and glycogen accumulation in brown adipose tissue. *Am J Physiol Endocrinol Metab*, **288**, E381-E387.

Ramos SG, Montenegro AP, Goissis G, Rossi MA (1994). Captopril reduces collagen and mast cell and eosinophil accumulation in pig serum-induced rat liver fibrosis. *Pathol Int*, **44**, 655-661.

Ramtohul YK, Black C, Chan CC, Crane S, Guay J, Guiral S, Huang Z, Oballa R, Xu LJ, Zhang L, Li CS (2010). SAR and optimization of thiazole analogs as potent stearoyl-CoA desaturase inhibitors. *Bioorg Med Chem Lett*, **20**, 1593-7.

Ran J, Hirano T, Adachi M (2004a). Angiotensin II type 1 receptor blocker ameliorates overproduction and accumulation of triglyceride in the liver of Zucker fatty rats. *Am J Physiol Endocrinol Metab*, **287**, E227–E232.

Ran J, Hirano T, Adachi M (2004b). Chronic ANG II infusion increases plasma triglyceride level by stimulating hepatic triglyceride production in rats. *Am J Physiol Endocrinol Metab*, **287**, E955–E961.

Ray PE, Aguilera G, Kopp JB, Horikoshi S, Klotman PE (1991). Angiotensin II receptor-mediated proliferation of cultured human fetal mesangial cells. *Kidney Int*, **40**, 764-771.

Rinella ME, Elias MS, Smolak RR, Fu T, Borensztajn J, Green RM (2008). Mechanisms of hepatic steatosis in mice fed a lipogenic methionine choline-deficient diet. *J Lipid Res*, **49**, 1068-1076.

Rizki G, Arnaboldi L, Gabrielli B, Yan J, Lee GS, Ng RK, Turner SM, Badger TM, Pitas RE, Maher JJ (2006). Mice fed a lipogenic methionine-choline-deficient diet develop hypermetabolism coincident with hapatic suppresion of SCD-1. *J Lipid Res*, **47**, 2280-2290.

Rong X, Li Y, Ebihara K, Zhao M, Kusakabe T, Tomita T, Murray M, Nakao K (2010). Irbesartan treatment up-regulates hepatic expression of PPARalpha and its target genes in obese Koletsky (fa(k)/fa(k)) rats: a link to amelioration of hypertriglyceridaemia. *Br J Pharmacol*, **160**, 1796–1807.

Sampath H, Flowers MT, Liu X, Paton CM, Sullivan R, Chu K, Zhao M, Ntambi JM (2009). Skin-specific deletion of stearoyl-CoA desaturase-1 alters skin lipid composition and protects mice from high fat diet-induced obesity. *J Biol Chem*, **284**, 19961-73.

Sampath H, Ntambi JM (2011). The role of stearoyl-CoA desaturase in obesity, insulin resistance and inflammation. *Ann NY Acad Sci*, **1243**, 47-53.

Sanyal AJ, Chalasani N, Kowdley KV, McCullough A, Diehl AM, Bass NM, Neuschwander-Tetri BA, Lavine JE, Tonascia J, Unalp A, Van Natta M, Clark J, Brunt EM, Kleiner DE, Hoofnagle JH, Robuck PR; NASH CRN (2010). Pioglitazone, vitamin E, or placebo for nonalcoholic steatohepatitis. *N Engl J Med*, **362**, 1675–1685.

Satapathy SK, Sakhuja P, Malhotra V, Sharma BC, Sarin SK (2006). Beneficial effects of pentoxifylline on hepatic steatosis, fibrosis and necroinflammation in patients with non-alcoholic steatohepatitis. *J Gastroenterol Hepatol*, **22**, 634–638.

Schneider AW, Kalk JF, Klein CP (1999). Effect of losartan, an angiotensin II receptor antagonist, on portal pressure in cirrhosis. *Hepatology*, **29**, 334-339.

Sun Y, Zhang J, Zhang JQ, Ramires FJ (2000). Local angiotensin II and transforming growth factor beta1 in renal fibrosis of rats. *Hypertension*, **35**, 1078-1084.

Terashima H, Kato M, Yasumo H, Tsuchida H, Mizuno M, Sada T (2010). A sensitive short-term evaluation of antifibrotic effects using newly established type I collagen reporter transgenic rats. *Am J Physiol*, **299**, F792-F801.

Tharaux PL, Chatziantoniou C, Fakhouri F, Dussaule JC (2000). Angiotensin II activates collagen I gene through a mechanism involving the MAP/ER kinase pathway. *Hypertension*, **36**, 330-336.

Torres DM, Harrison SA (2008). Diagnosis and therapy of nonalcoholic steatohepatitis. *Gastroenterology*, **134**, 1682-1698.

Trauner M, Arrese M, Wagner M (2010). Fatty liver and lipotoxicity. *Biochim Biophys Acta*, **1801**, 299-310.

Unger T (2002). The role of the renin–angiotensin system in the development of cardiovascular disease. *Am J Cardiol*, **89**, 3A–9A.

Uto Y, Ogata T, Kiyotsuka Y, Ueno Y, Miyazawa Y, Kurata H, Deguchi T, Watanabe N, Konishi M, Okuyama R, Kurikawa N, Takagi T, Wakimoto S, Osumi J (2010). Novel benzoylpiperidine-based stearoyl-CoA desaturase-1 inhibitors: Identification of 6-[4-(2-methylbenzoyl)piperidin-1-yl] pyridazine-3-carboxylic acid (2-hydroxy-2-pyridin-3-ylethyl)amide and its plasma triglyceride-lowering effects in Zucker fatty rats. *Bioorg Med Chem Lett*, **20**, 341-345.

Uto Y, Ogata T, Konishi M, Ueno Y, Kiyotsuka Y, Miyazawa Y, Kurata H, Ohsumi J. 2011 年 5 月 23 日. 日本ケミカルバイオロジー学会第 6 回年会. P-068; Benzoylpiperidine-based SCD inhibitors as lipid metabolism modulators.

Weber H, Taylor DS, Molloy CJ (1994). Angiotensin II induces delayed mitogenesis and cellular proliferation in rat aortic smooth muscle cells. *J Clin Invest*, **93**, 788-798.

Weber KT (1997). Fibrosis, a common pathway to organ failure: angiotensin II and tissue repair. *Semin Nephrol*, **17**, 467-491.

Williams EJ, Gaça MD, Brigstock DR, Arthur MJ, Benyon RC (2000). Increased expression of connective tissue growth factor in fibrotic human liver and in activated hepatic stellate cells. *J Hepatol*, **32**, 754-761.

Wolf G, Haberstroh U, Neilson EG (1992). Angiotensin II stimulates the proliferation and biosynthesis of type I collagen in cultured murine mesangial cells. *Am J Pathol*, **140**, 95-107.

Yata Y, Gotwals P, Koteliansky V, Rockey DC (2002). Dose-dependent inhibition of hepatic fibrosis in mice by a TGF-β soluble receptor: implications for antifibrotic therapy. *Hepatology*, **35**, 1022-1030.

Yokohama S, Yoneda M, Haneda M, Okamoto S, Okada M, Aso K, Hasegawa T, Tokusashi Y, Miyokawa N, Nakamura K (2004). Therapeutic efficacy of an angiotensin II receptor antagonist in patients with nonalcoholic steatohepatitis. *Hepatology*, **40**, 1222–1225.

Yokohama S, Tokusashi Y, Nakamura K, Tamaki Y, Okamoto S, Okada M, Aso K, Hasegawa T, Aoshima M, Miyokawa N, Haneda M, Yoneda M (2006). Inhibitory effect of angiotensin II receptor antagonist on hepatic stellate cell activation in non-alcoholic steatohepatitis. *World J Gastroenterol*, **12**, 322–326.

Yokozawa J, Sasaki T, Ohwada K, Sasaki Y, Ito JI, Saito T, Kawata S (2009). Down-regulation of hepatic stearoyl-CoA desaturase 1 expression by angiotensin II receptor blocker in the obese fa/fa Zucker rat: possible role in amelioration of insulin resistance and hepatic steatosis. *J Gastroenterol*, **44**, 583–591.

Yoshiji H, Kuriyama S, Yoshii J, Ikenaka Y, Noguchi R, Nakatani T, Tsujinoue H, Fukui H (2001). Angiotensin-II type 1 receptor interaction is a major regulator for liver fibrosis development in rats. *Hepatology*, **34**, 745-750.

Yoshiji H, Yoshii J, Ikenaka Y, Noguchi R, Tsujinoue H, Nakatani T, Imazu H, Yanase K, Kuriyama S, Fukui H (2002). Inhibition of rennin-angiotensin system attenuates liver enzyme-altered preneoplastic lesions and fibrosis development in rats. *J Hepatol*, **37**, 22-30.

Younossi ZM, Diehl AM, Ong JP (2002). Nonalcoholic fatty liver disease: an agenda for clinical research. *Hepatology*, **35**, 746-752.

Zhang S, Wang J, Liu Q, Harnish DC (2009). Farnesoid X receptor agonist WAY-362450 attenuates liver inflammation and fibrosis in murine model of non-alcoholic steatohepatitis. *J Hepatol*, **51**, 380-388.

Tables

Table 1 Sequences of primers and probes used in real-time PCR analysis

Collagen 1a1		
	Forward primer	5'-CTCCCAGCGGTGGTTATGAC-3'
	Reverse primer	5'-TGCTGGCTCAGGCTCTTGA-3'
	Probe	5'-*FAM*-AAGATGGTGGCCGTTACTACCGGGC-*TAMRA*-3'
α-Smooth muscle actin (α-SMA)		
	Forward primer	5'-CAACTGGTATTGTGCTGGACTCTG-3'
	Reverse primer	5'-CTCCTTGATGTCACGGACGATCT-3'
	Probe	5'-*FAM*-AGATGGCGTGACTCACAACGTGCCT-*TAMRA*-3'
Connective tissue growth factor (CTGF)		
	Forward primer	5'-CAATACCTTCTGCAGGCTGGA-3'
	Reverse primer	5'-TTAGCCCGGTAGGTCTTCACA-3'
	Probe	5'-*FAM*-TGCATCCGGACGCCTAAAATTGCCA-*TAMRA*-3'
Monocyte chemotactic protein-1 (MCP-1)		
	Forward primer	5'-CTTCACAGTTGCTGCCTGTAGC-3'
	Reverse primer	5'-AGTGAATGAGTAGCAGCAGGTGAG-3'
	Probe	5'-*FAM*-TGTCTCAGCCAGATGCAGTTAATGCCC-*TAMRA*-3'
Stearoyl-CoA desaturase-1 (SCD-1)		
	Forward primer	5'-CCGCTGGCACATCAACTTCA-3'
	Reverse primer	5'-AAACTTTTTTCCGGTCGTAAGCC-3'
	Probe	5'-*FAM*-CACGTTCTTCATCGACTGCATGGCTG-*TAMRA*-3'

The sequences of primers and probes for each gene used in present study are indicated. *FAM*; 6-carboxyfluorescein, *TAMRA*; 6-carboxytetramethylrhodamine.

Table 2 Effects of an SCD-1 Inhibitor on body weight and liver weight of MCD rats

			Compound A (mg/kg)	
	Control	MCD	30	100
Body weight gain (g)	9.6 ± 5.6	-76.4 ± 2.6**	-80.8 ± 5.1	-89.4 ± 4.3
Liver weight (g)	9.41 ± 0.08	6.56 ± 0.23**	6.35 ± 0.4	6.17 ± 0.22
Liver weight (g/100 g of body weight)	3.57 ± 0.06	3.59 ± 0.08	3.64 ± 0.18	3.74 ± 0.08

Rats were treated as shown in Materials and Methods. Control, vehicle-treated rats fed with control diets (n = 4); MCD, vehicle-treated rats fed with MCD diets (n = 8); compound A (30 and 100 mg/kg/day) was administered daily to rats fed with MCD diets (n = 5 and 4, respectively). Body weight was measured before and at 8 weeks after the first treatment, and body weight gain was calculated. Livers were removed and weighed at 8 weeks after the first treatment. Values are Means ± SE. ** $p < 0.01$ vs. control (by t-test).

Table 3 Comparison of MCD and BDL models

		Metabolic disorders	Hepatic steatosis	Liver injury Inflammation	Fibrosis
MCD model	Fatty liver-based NASH models	Yes	Yes	Yes	Yes
BDL model	Pure fibrosis models	No	No	Yes	Yes

MCD; methionine and choline-deficient, BDL; bile duct ligation

Table 4 Effects of ARB on survival rate, final body weight and liver weight

	Sham	BDL	BDL + ARB
Survival rate	100% (n = 5)	80% (n = 10)	70% (n = 10)
Final body weight (g)	304 ± 7	275 ± 8*	250 ± 15
Liver weight (g/100 g of body weight)	3.41 ± 0.07	6.06 ± 0.15**	5.46 ± 0.24$^{\#\#}$

Rats were treated as described in Materials and Methods. Sham, sham-operated rats receiving the vehicle; BDL, bile duct-ligated rats receiving the vehicle; BDL+ARB, bile duct ligation followed by 1 mg/kg/day of olmesartan treatment. Survival rate was calculated during the treatment of ARB (from Day 7 to Day 21). Final body weight and liver were weighed at 3 weeks after surgery. Values are Means ± SE. * $p < 0.05$,** $p < 0.01$ vs. sham, $^{\#\#}$ $p < 0.01$ vs. BDL.

Figures

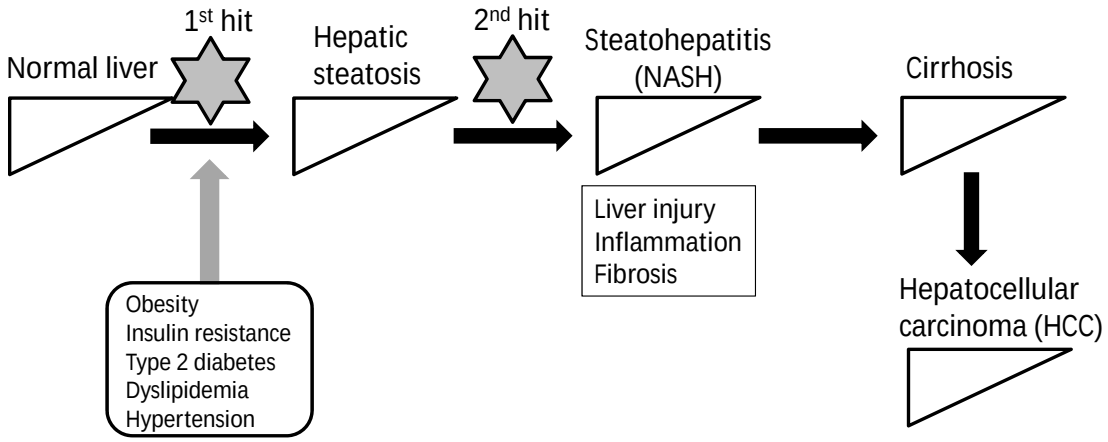

Figure 1 "Two hit theory" in onset and progression of NASH. NASH is thought to develop in a two-step process. The "first hit" is the lipid accumulation in the liver, which is caused by obesity, insulin resistance and other metabolic disorders. Subsequently the "second hit" stimuli lead to liver injury, inflammation and fibrosis.

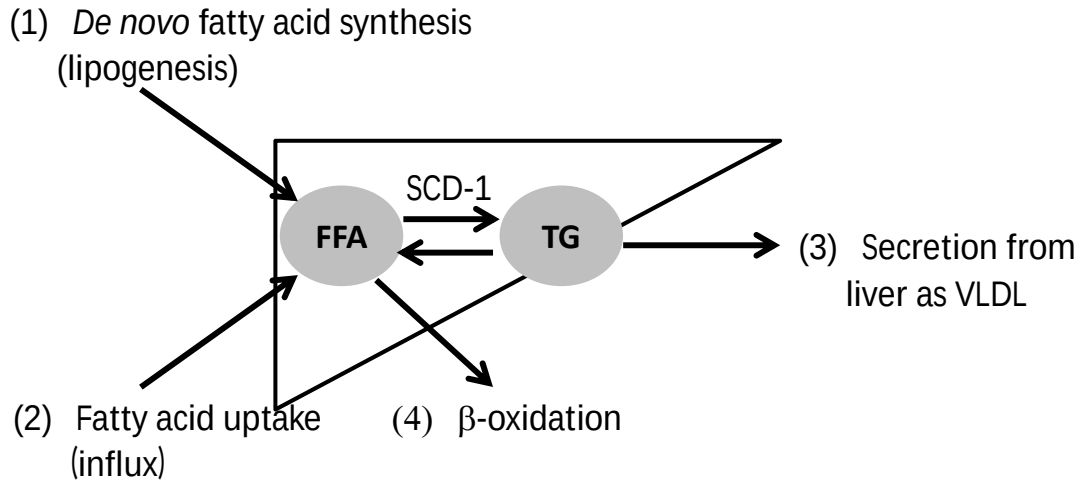

Figure 2 Regulation of lipid content in liver. Liver lipid levels were regulated by four mechanisms as shown in (1) to (4). In NASH/NAFLD patients, (1) and (2) are generally up-regulated. FFA: fatty acid, TG; triglyceride, VLDL; very low density lipoprotein

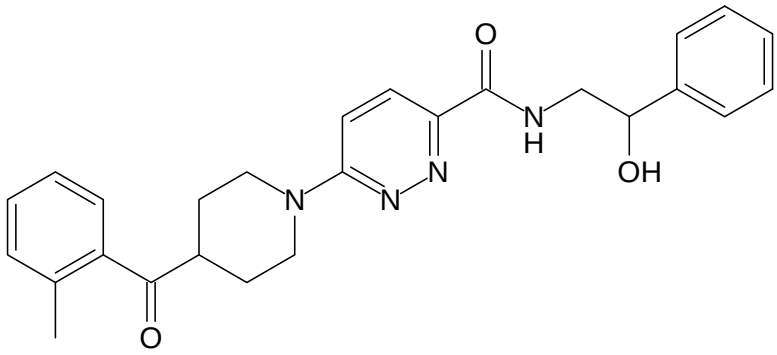

Figure 3 Structure of an SCD-1 inhibitor, compound A.

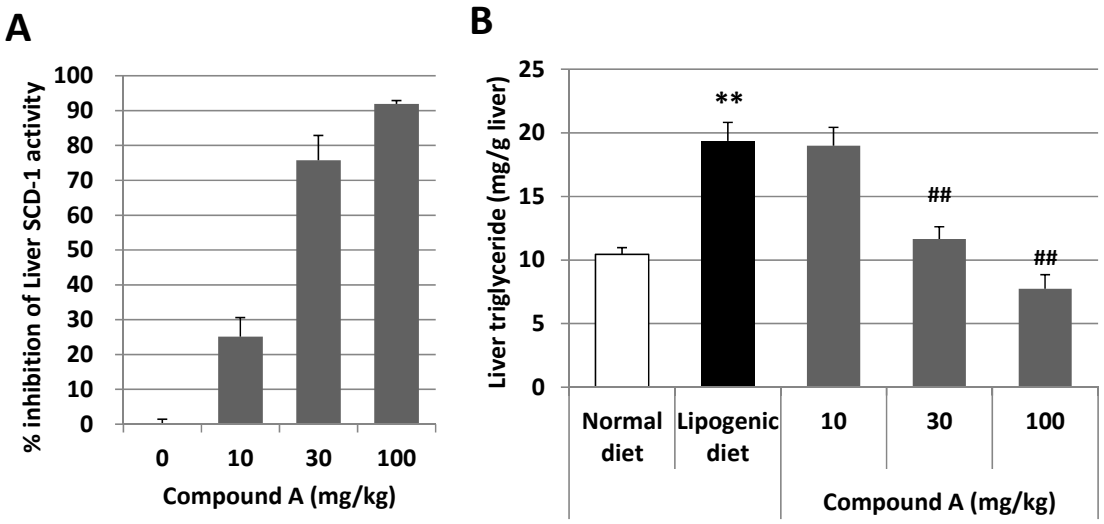

Figure 4 Effects of compound A on SCD-1 activity (**A**) and triglyceride levels (**B**) in the liver of mice fed with lipogenic diets. (**A**) Compound A was administered once at doses of 10, 30 and 100 mg/kg to mice fed with lipogenic diets (n = 2). Liver SCD-1 activity was measured as shown in Materials and Methods. (**B**) Compound A was administered once-daily for 7 days at doses of 10, 30 and 100 mg/kg to mice fed with lipogenic diets (n = 6). Liver triglyceride content was measured as shown in Materials and Methods. Values are Means + SE. ** $p < 0.01$ vs. normal diet (by Student's t-test), $^{\#\#}$ $p < 0.01$ vs. lipogenic diets (by Dunnett's test).

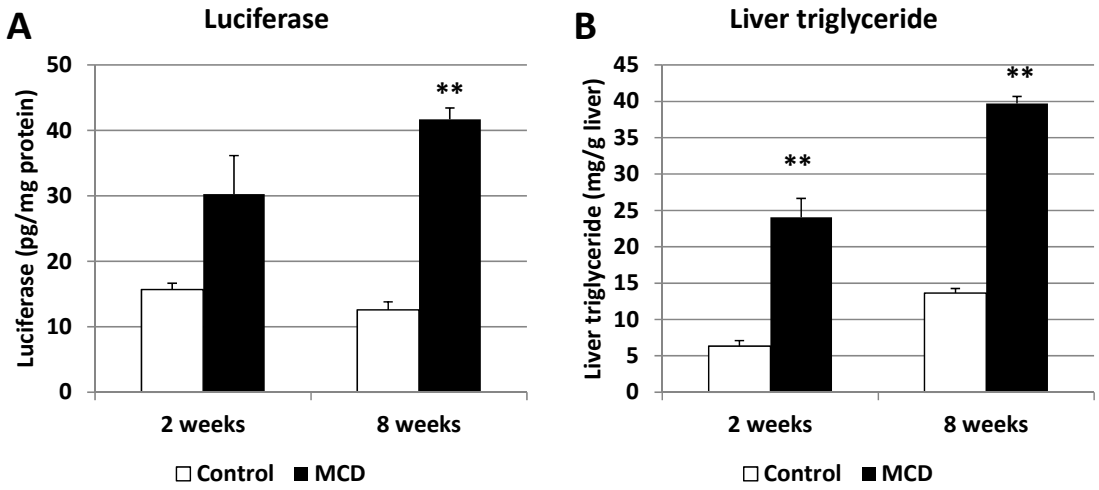

Figure 5 Luciferase (**A**) and triglyceride content (**B**) in the liver of MCD rats. Rats were treated as described in Materials and Methods. Control, vehicle-treated rats fed with control diets (n = 5 for each time point); MCD, vehicle-treated rats fed with MCD diets (n = 5 for each time point). Liver samples were prepared at indicated times after starting feeding of MCD diets. Values are Means + SE. ** $p < 0.01$ vs. control (by Student's t-test).

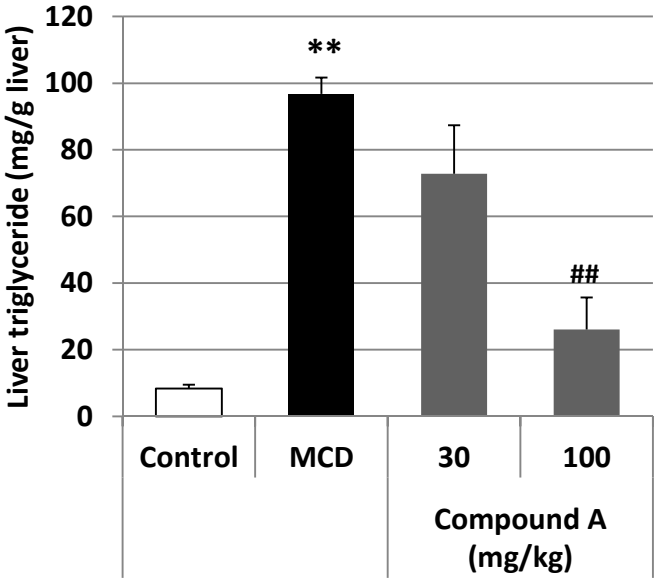

Figure 6 Effects of SCD-1 inhibitor on liver triglyceride levels in MCD rats. Rats were treated as shown in Materials and Methods. Control, vehicle-treated rats fed with control diets (n = 4); MCD, vehicle-treated rats fed with MCD diets (n = 8); an SCD-1 inhibitor, compound A (30 and 100 mg/kg/day) was administered daily to rats fed with MCD diets (n = 5 and 4, respectively). Livers were prepared at 8 weeks after the first treatment. Values are Means + SE. ** $p < 0.01$ vs. control (by Student's t-test), $^{\#\#}$ $p < 0.01$ vs. MCD (by Dunnett's test).

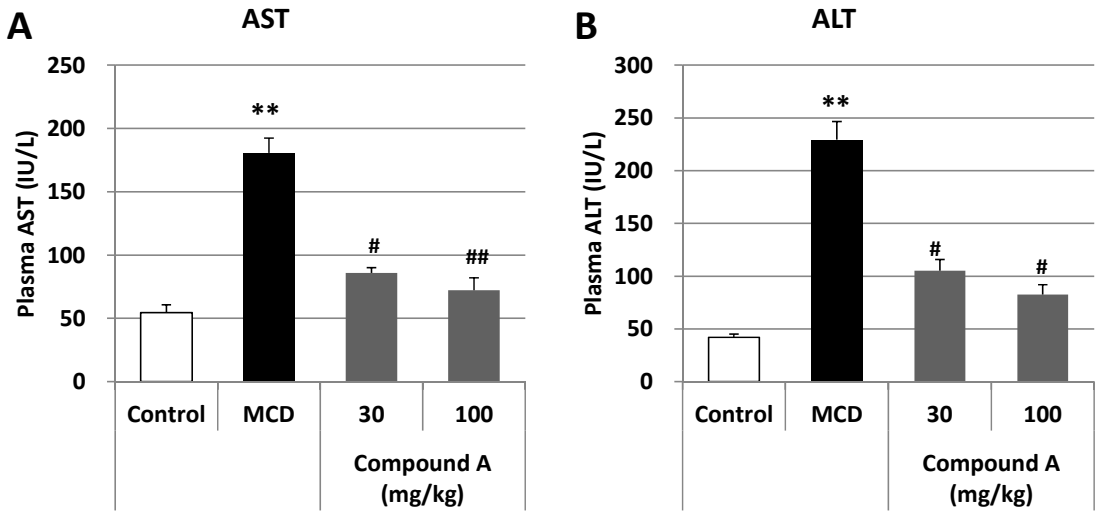

Figure 7 Effects of SCD-1 inhibitor on plasma AST (**A**) and ALT (**B**) levels in MCD rats. Rats were treated as shown in Materials and Methods. Control, vehicle-treated rats fed with control diets (n = 4); MCD, vehicle-treated rats fed with MCD diets (n = 8); an SCD-1 inhibitor, compound A (30 and 100 mg/kg/day) was administered daily to rats fed with MCD diets (n = 5 and 4, respectively). Plasma samples were prepared at 8 weeks after the first treatment. Values are Means + SE. ** $p < 0.01$ vs. control (Student's t-test), $^{\#}$ $p < 0.05$, $^{\#\#}$ $p < 0.01$ vs. MCD (Dunnett's test).

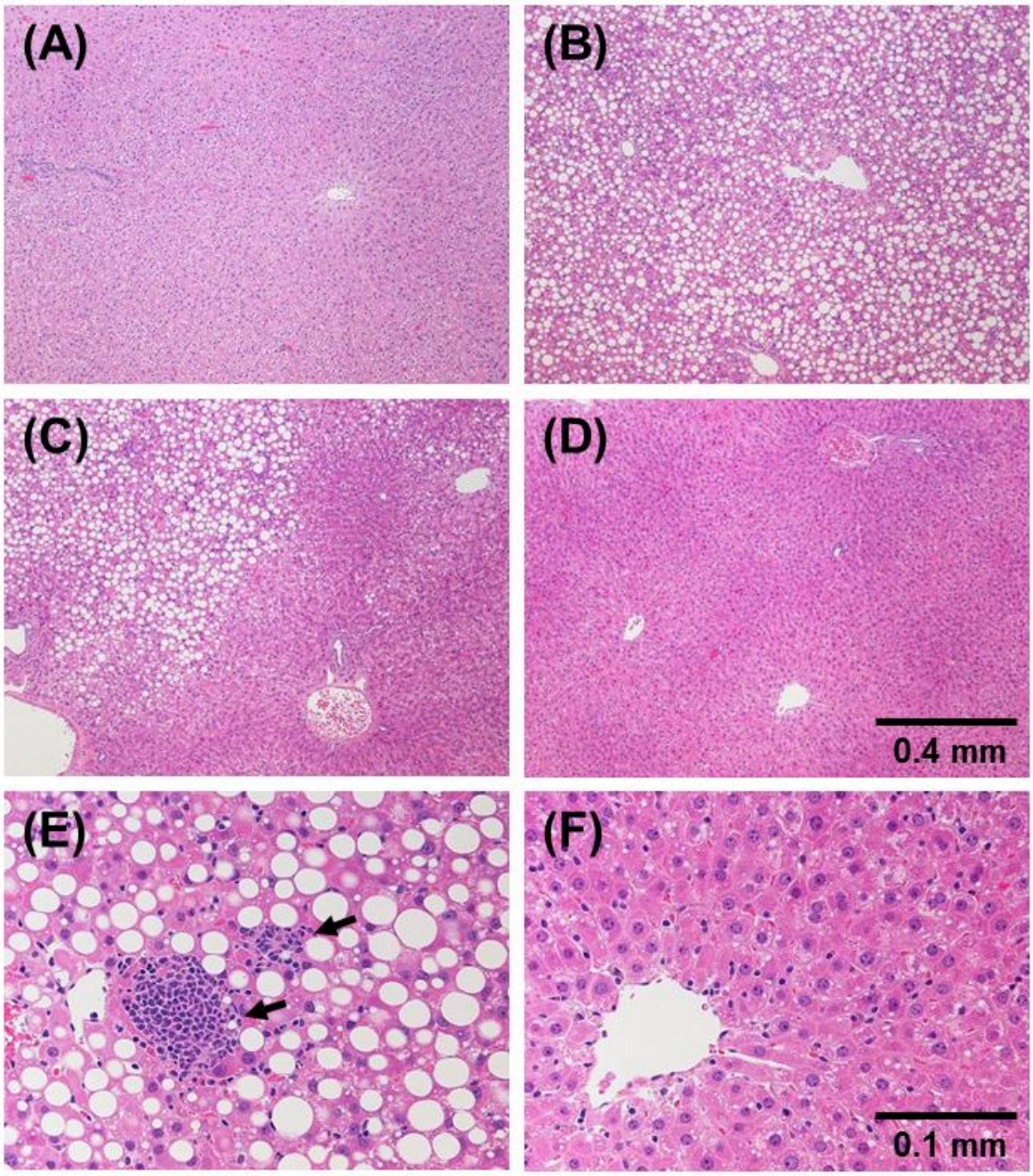

(Figure 8)

Figure 8 Histological analysis of liver of SCD-1 inhibitor-treated MCD rats. Rats were treated as shown in Materials and Methods. (**A**) Control, vehicle-treated rats fed with control diets; (**B**) and (**E**) MCD, vehicle-treated rats fed with MCD diets; (**C**) an SCD-1 inhibitor, compound A 30 mg/kg/day; (**D**) and (**F**) compound A 100 mg/kg/day; compound A was administered daily to rats fed with MCD diets. Liver sections were prepared at 8 weeks after the first treatment, and performed by hematoxylin-eosin staining. Representative sections of rats in each group are shown. Arrows indicate inflammatory cell infiltration. Scale of bars in (**A**) to (**D**) indicate 0.4 mm and 0.1 mm in (**E**) and (**F**).

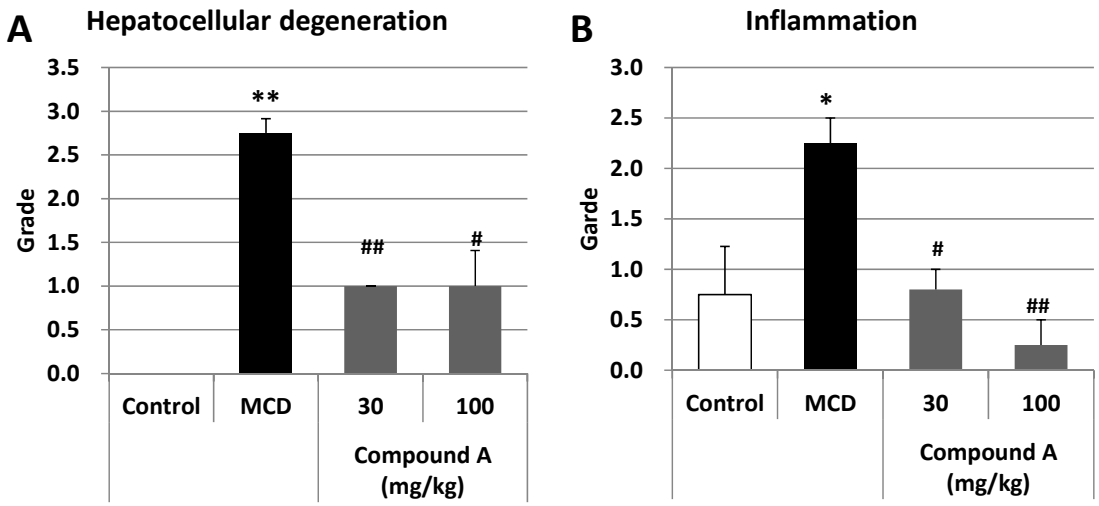

Figure 9 The scores of hepatocellular degeneration (**A**) and inflammation (**B**) in the liver of SCD-1 inhibitor-treated MCD rats. Rats were treated as shown in Materials and Methods. Control, vehicle-treated rats fed with control diets (n = 4); MCD, vehicle-treated rats fed with MCD diets (n = 8); an SCD-1 inhibitor, compound A (30 and 100 mg/kg/day) was administered daily to rats fed with MCD diets (n = 5 and 4, respectively). Liver sections were prepared at 8 weeks after the first treatment, and performed by hematoxylin-eosin staining. The degree of hepatocellular degeneration and inflammation were scored as follows: 0, none; 1, slight; 2, mild; 3, moderate. Inflammation was indicated as the sum (0 to 6) of portal inflammation (score: 0 to 3) and lobular inflammation (score: 0 to 3). Values are Means + SE * $p < 0.05$, ** $p < 0.01$ vs. control (by Student's t-test), $^{\#}$ $p < 0.05$, $^{\#\#}$ $p < 0.01$ vs. MCD (by Dunnett's test).

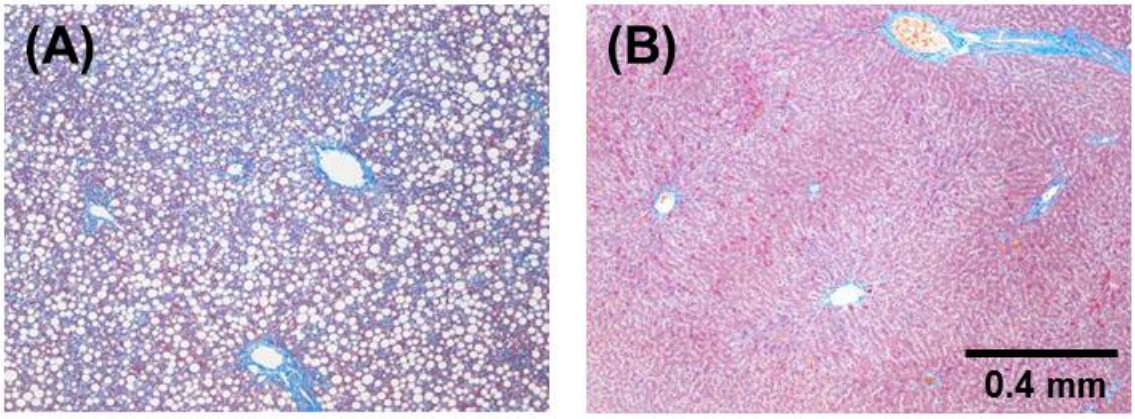
(A)
(B)
0.4 mm

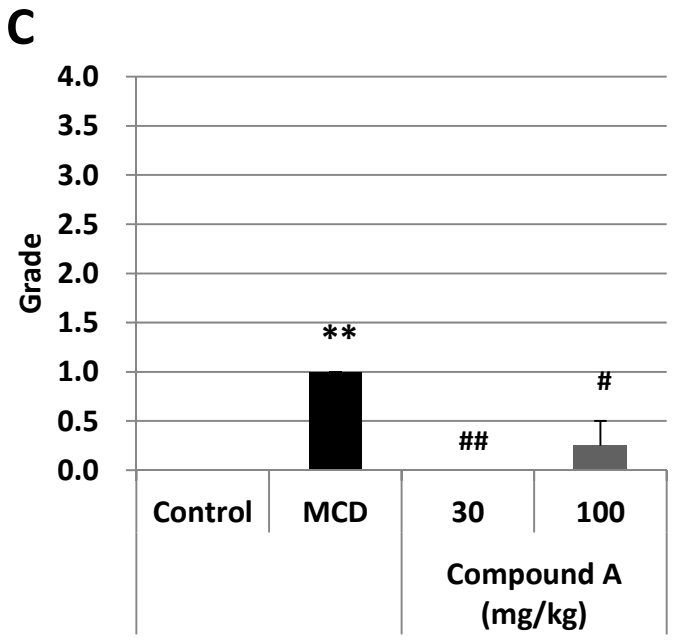
C
Grade
4.0
3.5
3.0
2.5
2.0
1.5
1.0
0.5
0.0
**
#
##
Control
MCD
30
100
Compound A
(mg/kg)

(Figure 10)

Figure 10 Masson-trichrome staining of liver in SCD-1 inhibitor-treated MCD rats. Rats were treated as shown in Materials and Methods. Control, vehicle-treated rats fed with control diets (n = 4); MCD, vehicle-treated rats fed with MCD diets (n = 8); an SCD-1 inhibitor, compound A (30 and 100 mg/kg/day) was administered daily to rats fed with MCD diets (n = 5 and 4, respectively). Liver sections were prepared at 8 weeks after the first treatment, and performed by Masson-trichrome staining. Representative sections of rats in MCD (**A**) and compound A 100 mg/kg/day (**B**) are shown. Fibrotic area is stained as blue. Bar indicates 0.4 mm. (**C**) fibrosis was scored as follows: 1, pericellular and perivenular fibrosis; 2, focal bridging fibrosis; 3, bridging fibrosis with lobular distortion; 4, cirrhosis. Values are Means + SE. ** $p < 0.01$ vs. control (by Student's t-test), $^{\#}$ $p < 0.05$, $^{\#\#}$ $p < 0.01$ vs. MCD (by Dunnett's test).

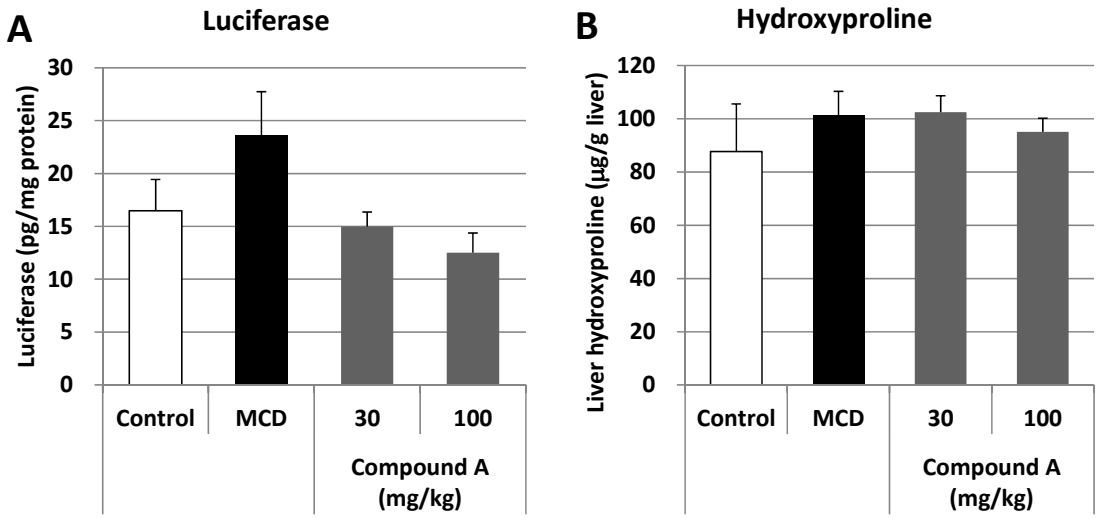

Figure 11 Effects of SCD-1 inhibitor on promoter activity of collagen 1a1 (**A**) and hydroxyproline content (**B**) in the liver of MCD rats. Rats were treated as shown in Materials and Methods. Control, vehicle-treated rats fed with control diets (n = 4); MCD, vehicle-treated rats fed with MCD diets (n = 8); an SCD-1 inhibitor, compound A (30 and 100 mg/kg/day) was administered daily to rats fed with MCD diets (n = 5 and 4, respectively). Liver samples were prepared at 8 weeks after the first treatment. Values are Means + SE. All of the data were not statistically significant (by Student's t-test or Dunnett's test).

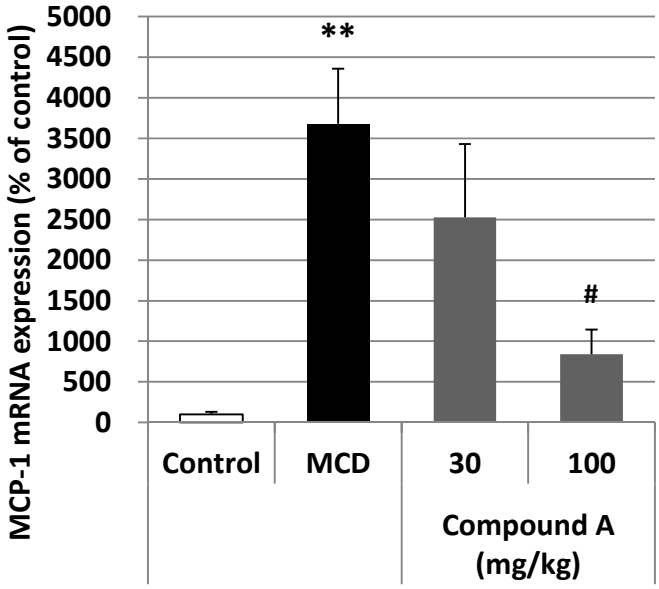

Figure 12 Effects of SCD-1 inhibitor on mRNA expression of MCP-1 in the liver of MCD rats. Rats were treated as shown in Materials and Methods. Control, vehicle-treated rats fed with control diets (n = 4); MCD, vehicle-treated rats fed with MCD diets (n = 8); an SCD-1 inhibitor, compound A (30 and 100 mg/kg/day) was administered daily to rats fed with MCD diets (n = 5 and 4, respectively). Liver samples were prepared at 8 weeks after the first treatment. Values are Means + SE. ** $p < 0.01$ vs. control (by Student's t-test), $^{\#}$ $p < 0.05$ vs. MCD (by Dunnett's test).

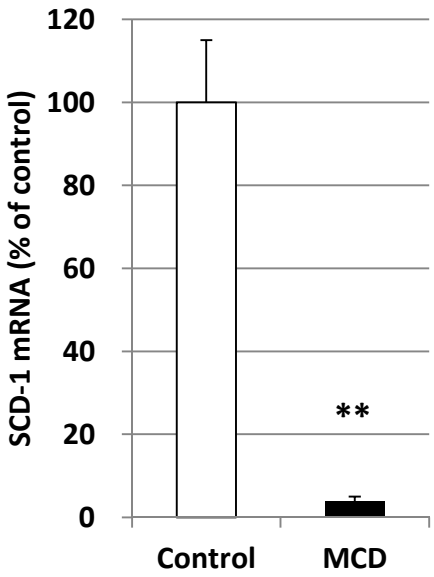

Figure 13 Effects of feeding of MCD diets on SCD-1 mRNA expressions in the liver of rats. Rats were treated as shown in Materials and Methods. Control, vehicle-treated rats fed with control diets (n = 4); MCD, vehicle-treated rats fed with MCD diets (n = 8). Liver samples were prepared after 8 weeks feeding of MCD diets. Values are Means + SE ** $p < 0.01$ vs. control (by Student's t-test).

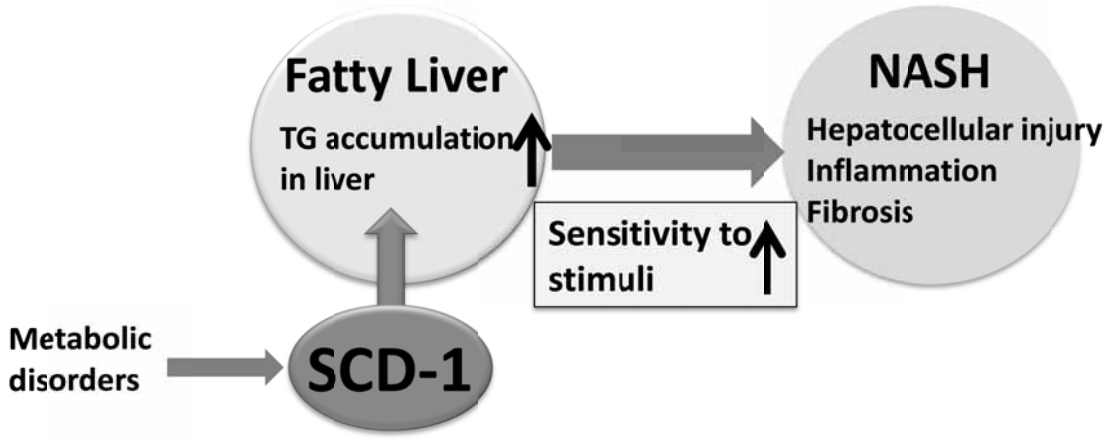

Figure 14 Summary of the role of SCD-1 in the onset process of NASH. SCD-1 causes triglyceride accumulation in the liver and consequently increases sensitivity to the onset of NASH pathology including liver injury, inflammation and fibrosis.

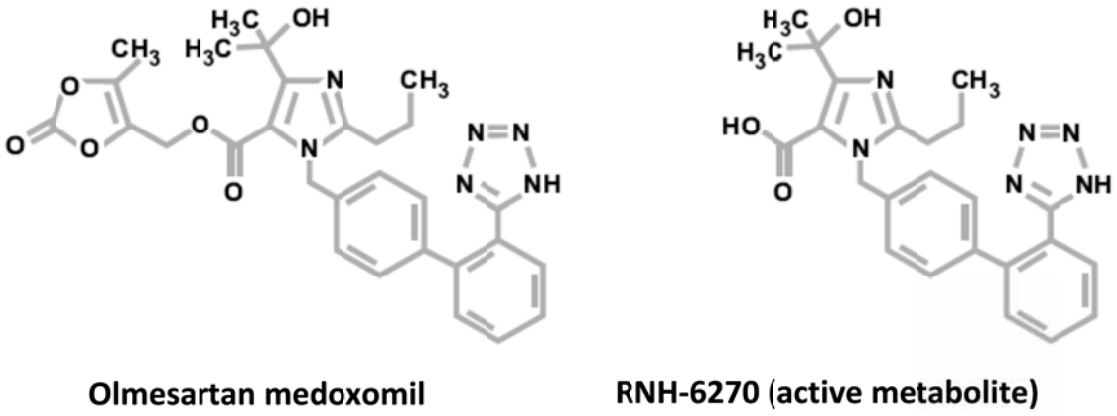

Figure 15 Chemical structures of olmesartan medoxomil and its active metabolite, RNH-6270.

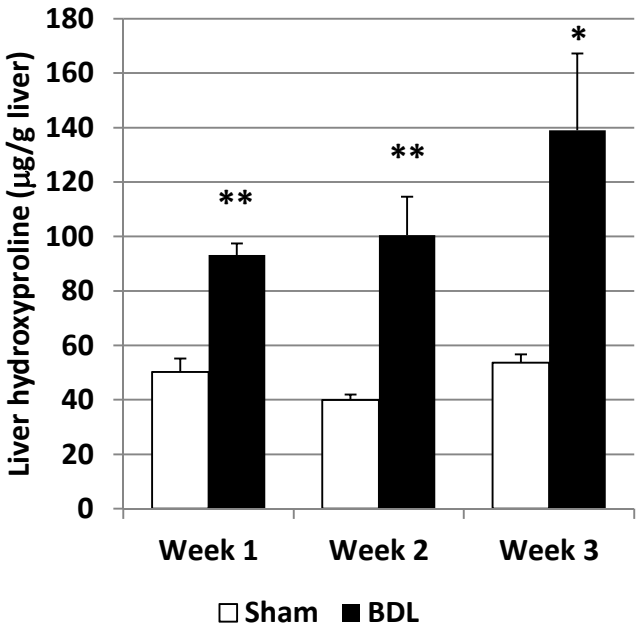

Figure 16 Time course of hydoxyproline content in the liver of BDL rats. Rats were treated as described in Materials and Methods. Sham, sham-operated rats receiving the vehicle (n = 3 to 5); BDL, bile duct-ligated rats receiving the vehicle (n = 3 to 6). Liver samples were prepared at indicated times after surgery. Values are Means + SE. * $p < 0.05$, ** $p < 0.01$ vs. sham (by Student's t-test).

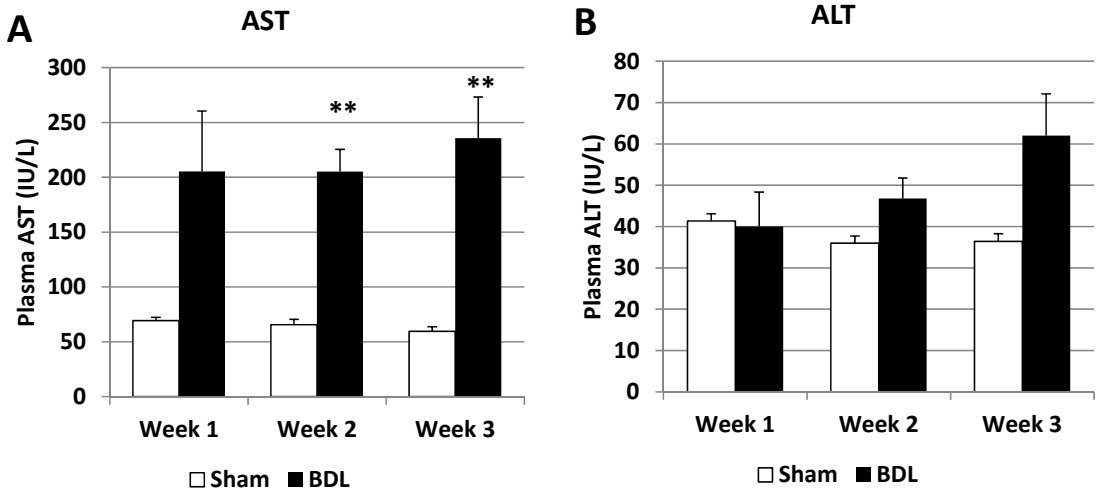

Figure 17 Time course of plasma AST (**A**) and ALT (**B**) levels in BDL rats. Rats were treated as described in Materials and Methods. Sham, sham-operated rats receiving the vehicle (n = 3 to 5); BDL, bile duct-ligated rats receiving the vehicle (n = 3 to 6). Plasma samples were prepared at indicated times after surgery. Values are Means + SE. ** $p < 0.01$ vs. sham (by Student's t-test).

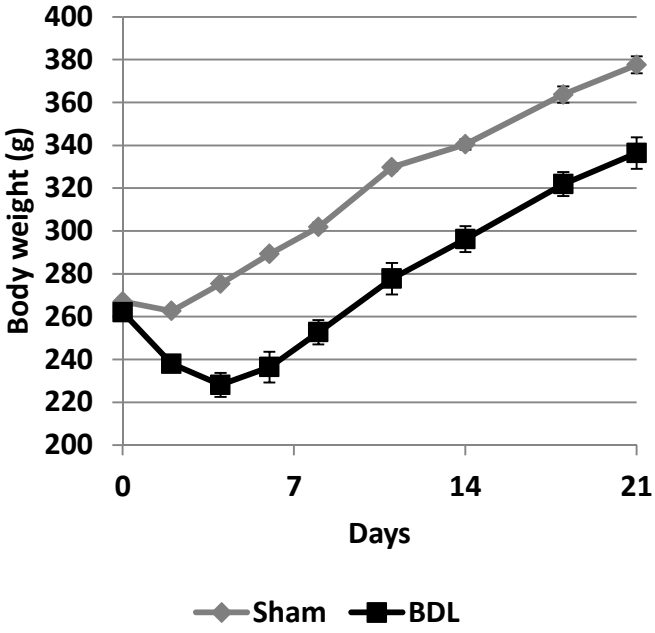

Figure 18 Time course of body weight change in BDL rats. Rats were treated as described in Materials and Methods. Sham, sham-operated rats receiving the vehicle (n = 5); BDL, bile duct-ligated rats receiving the vehicle (n = 5). Values are Means ± SE.

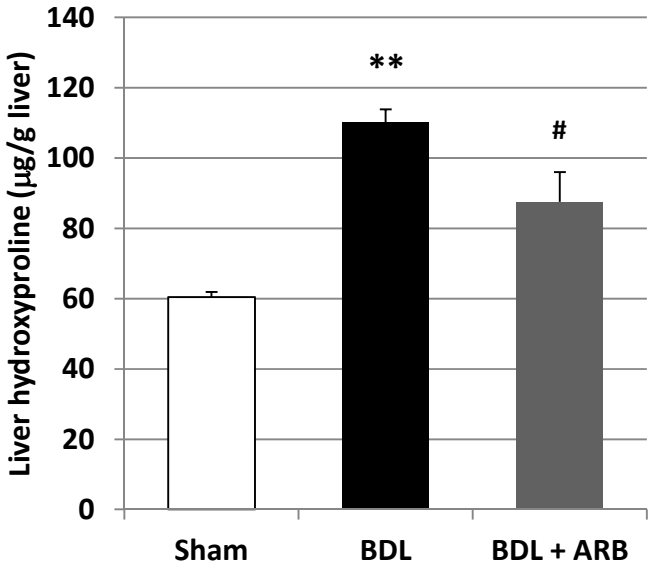

Figure 19 Effects of ARB on liver hydroxyproline content in BDL rats. Rats were treated as described in Materials and Methods. Sham, sham-operated rats receiving the vehicle (n = 5); BDL, bile duct-ligated rats receiving the vehicle (n = 8); BDL+ARB, bile duct ligation followed by 1 mg/kg/day of olmesartan treatment (n = 7). Liver samples were prepared at 3 weeks after surgery. Values are Means + SE. ** $p < 0.01$ vs. sham, $^{\#}$ $p < 0.05$ vs. BDL (by Student's t-test).

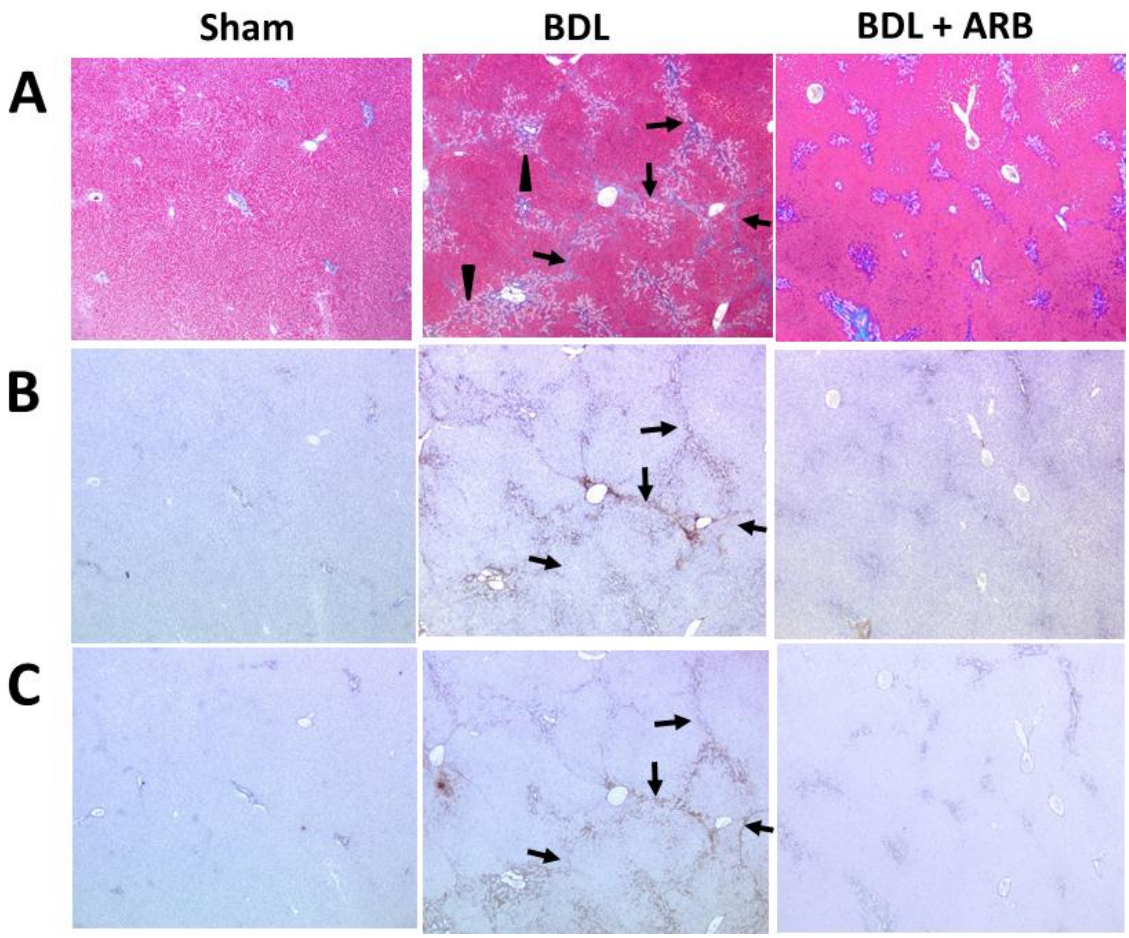

Figure 20 Histological analysis of the liver in ARB-treated BDL rats. Liver sections were examined by Masson-trichrome staining (**A**), immunohistochemical staining using antibodies against α-SMA (**B**) or AT1 receptor (**C**). Rats were treated as described in Materials and Methods. Sham, sham-operated rats receiving the vehicle; BDL, bile duct-ligated rats receiving the vehicle; BDL+ARB, bile duct ligation followed by 1 mg/kg/day of olmesartan treatment. Liver samples were prepared at 3 weeks after surgery. The three images on the left, in the middle and on the right are consecutive. Representative sections of rats in each group are shown. Arrowheads indicate the bile duct proliferation. Arrows indicate the site of fibrosis (**A**), the α-SMA-positive cells (**B**) and the AT1-positive cells (**C**), respectively. Original magnification ×25.

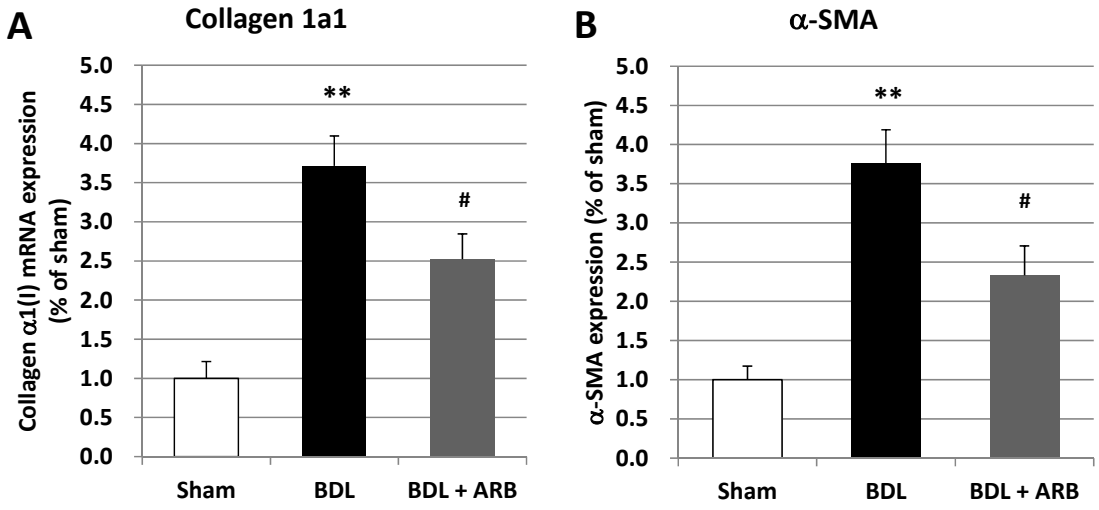

Figure 21 Effects of ARB on mRNA expression of collagen 1a1 (**A**) and α-SMA (**B**) in the liver of BDL rats. Rats were treated as described in Materials and Methods. Sham, sham-operated rats receiving the vehicle (n = 5); BDL, bile duct-ligated rats receiving the vehicle (n = 8); BDL+ARB, bile duct ligation followed by 1 mg/kg/day of olmesartan treatment (n = 7). Liver samples were prepared at 3 weeks after surgery. Values are Means + SE. ** $p < 0.01$ vs. sham, $^{\#}$ $p < 0.05$ vs. BDL (by Student's t-test).

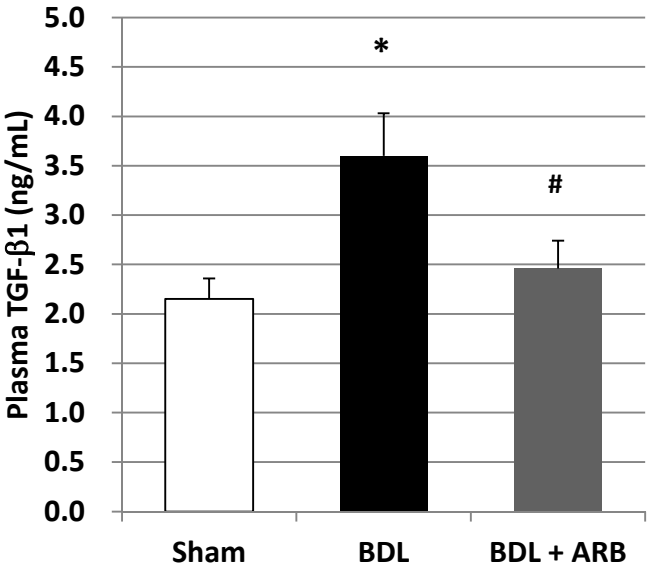

Figure 22 Effects of ARB on plasma TGF-β1 levels in BDL rats. Rats were treated as described in Materials and Methods. Sham, sham-operated rats receiving the vehicle (n = 5); BDL, bile duct-ligated rats receiving the vehicle (n = 8); BDL+ARB, bile duct ligation followed by 1 mg/kg/day of olmesartan treatment (n = 7). Plasma samples were prepared at 3 weeks after surgery. Values are Means + SE. * $p < 0.05$ vs. sham, $^{\#}$ $p < 0.05$ vs. BDL (by Student's t-test).

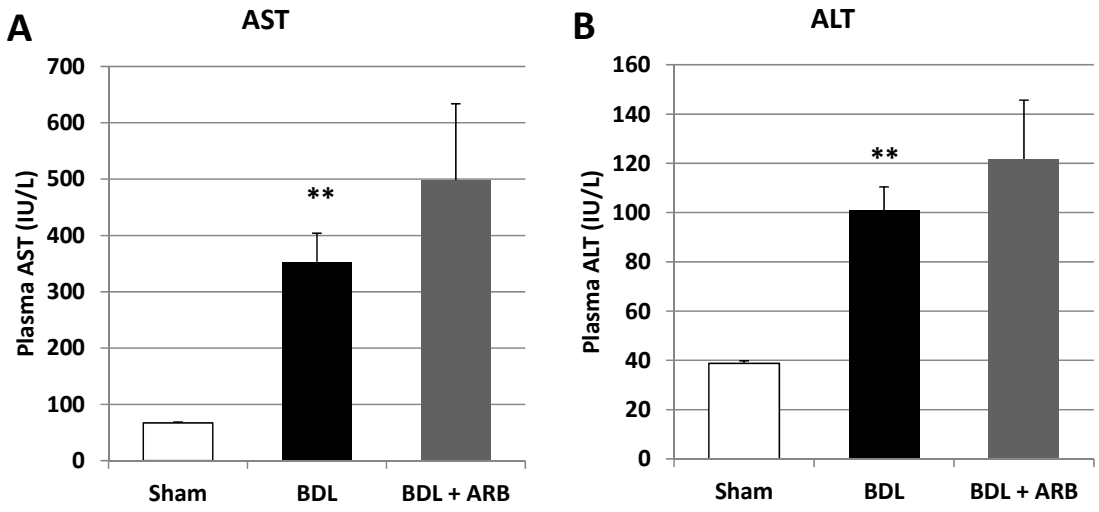

Figure 23 Effects of ARB on plasma AST (**A**) and ALT (**B**) levels in BDL rats. Rats were treated as described in Materials and Methods. Sham, sham-operated rats receiving the vehicle (n = 5); BDL, bile duct-ligated rats receiving the vehicle (n = 8); BDL+ARB, bile duct ligation followed by 1 mg/kg/day of olmesartan treatment (n = 7). Plasma samples were prepared at 3 weeks after surgery. Values are Means + SE. ** $p < 0.01$ vs. sham (by Student's t-test).

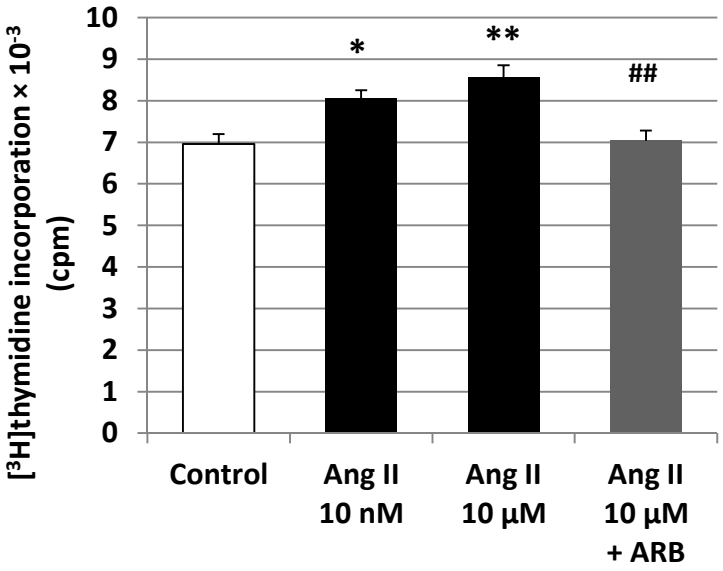

Figure 24 Effects of Ang II and ARB on proliferation in activated HSCs *in vitro*. HSCs were incubated with Ang II in the presence or absence of 10 μM RNH-6270 (ARB) in serum-free medium for 48 hr., and DNA synthesis was measured by calculating the amount of incorporated [^{3}H]thymidine into cells, as described in Materials and Methods. Values are means + SE of 8 separate experiments. * $p < 0.05$, ** $p < 0.01$ vs. control (by Dunnett's test); $^{\#\#}$ $p < 0.01$ vs. Ang II 10 μM (by Student's t-test).

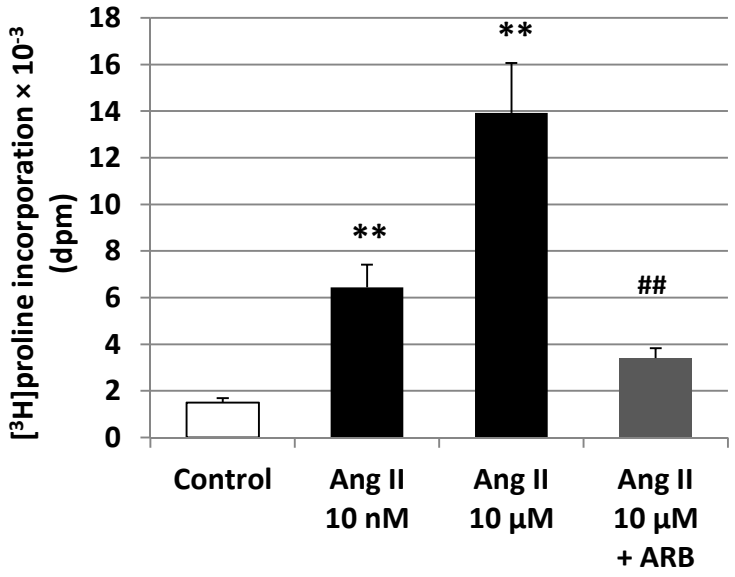

Figure 25 Effects of Ang II and ARB on collagen synthesis in activated HSCs *in vitro*. HSCs were incubated with Ang II in the presence or absence of 10 μM RNH-6270 (ARB) in serum-free medium for 48 hrs., and collagen synthesis was measured by calculating the amount of incorporated [^{3}H]proline, as described in Materials and Methods. Values are means + SE of 8 separate experiments. Statistical tests were performed with logarithmically transformed values. ** $p < 0.01$ vs. control (by Dunnett's test); $^{\#\#}$ $p < 0.01$ vs. Ang II 10 μM (by Student's t-test).

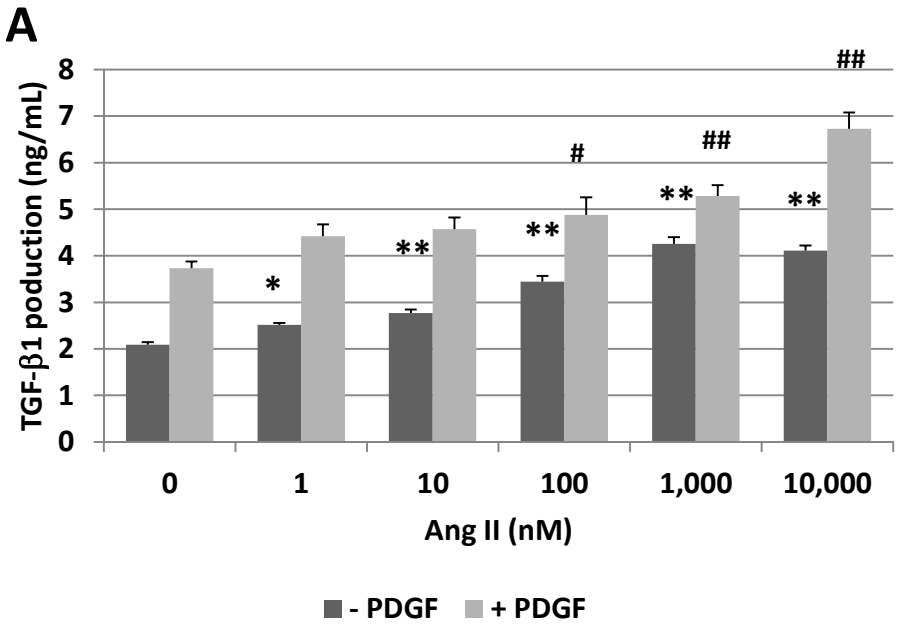
A
TGF-β1 poduction (ng/mL)
0
1
2
3
4
5
6
7
8
*
**
**
#
**
##
**
##
0
1
10
100
1,000
10,000
Ang II (nM)
- PDGF
+ PDGF

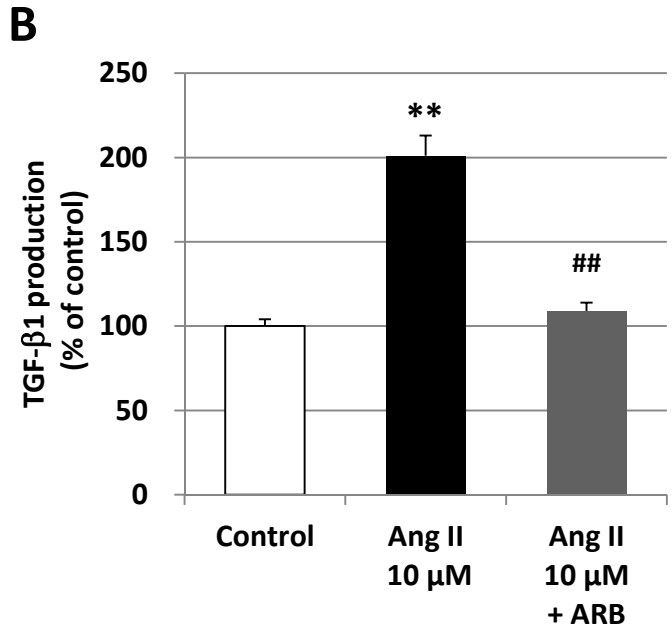
B
TGF-β1 production (% of control)
0
50
100
150
200
250
**
##
Control
Ang II 10 µM
Ang II 10 µM + ARB

(Figure 26)

Figure 26 Effects of Ang II and ARB on TGF-β1 production in activated HSCs *in vitro*. HSCs were incubated with Ang II in the presence or absence of 25 ng/mL PDGF (**A**) and in the presence or absence of 10 μM RNH-6270 (ARB) (**B**) in serum-free medium for 48 hrs. The collected culture supernatants were acidified, and then total TGF-β1 amount in the supernatants was measured as described in Materials and Methods. Values are means + SE of 8 separate experiments. (**A**) * $p < 0.05$, ** $p < 0.01$ vs. 0 nM Ang II without PDGF, $^{\#}$ $p < 0.05$, $^{\#\#}$ $p < 0.01$ vs. 0 nM Ang II with PDGF, (**B**) ** $p < 0.01$ vs. control (by Dunnett's test); $^{\#\#}$ $p < 0.01$ vs. Ang II 10 μM (by Student's t-test).

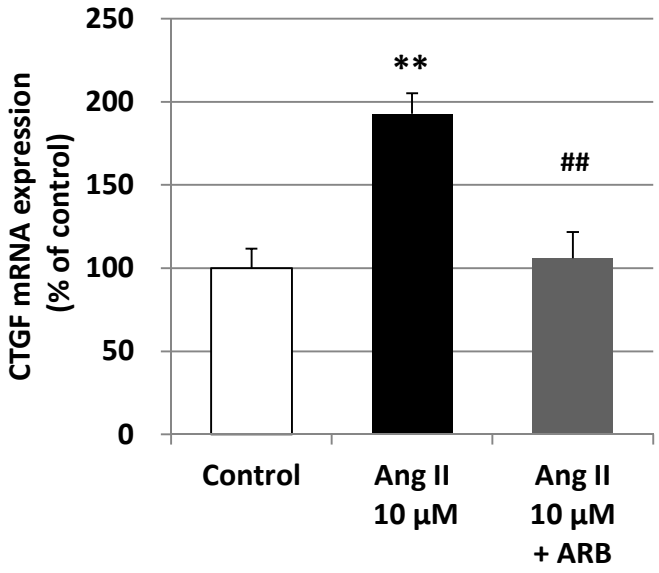

Figure 27 Effects of Ang II and ARB on mRNA expression of CTGF in activated HSCs *in vitro*. HSCs were incubated with Ang II in the presence or absence of 10 μM RNH-6270 (ARB) in serum-free medium for 48 hrs. Total RNA was extracted from cells, and mRNA expression was determined by TaqMan PCR analysis as described in Materials and Methods. RNA was normalized to that of GAPDH RNA. Values are means + SE of 5 separate experiments. ** $p < 0.01$ vs. control (by Student's t-test); $^{\#\#}$ $p < 0.01$ vs. Ang II 10 μM (by Dunnett's test).

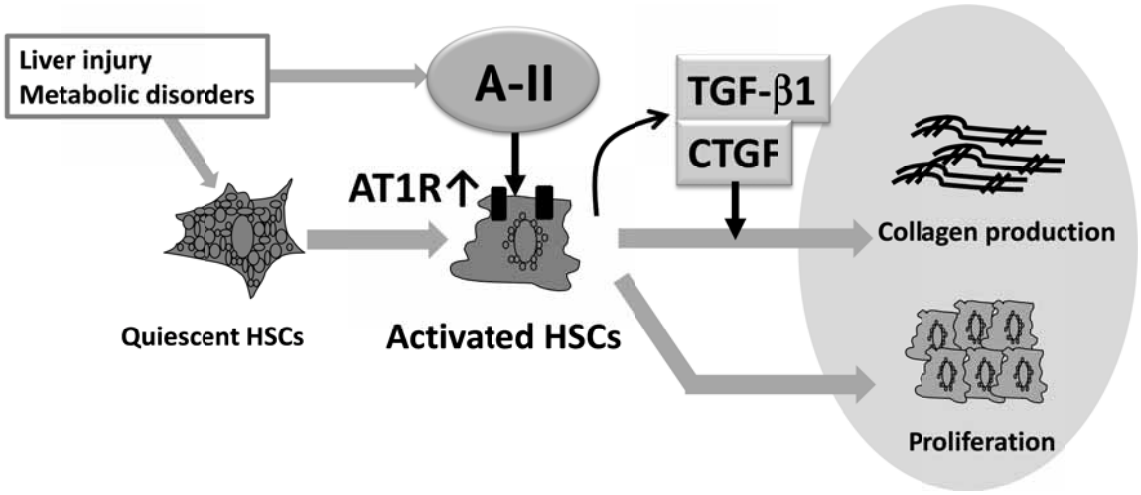

Figure 28 Summary of the role of Ang II in progression of liver fibrosis. Ang II stimulates proliferation and collagen synthesis in activated HSCs possibly through up-regulation of TGF-β1 and CTGF, consequently leads to the progression of liver fibrosis.

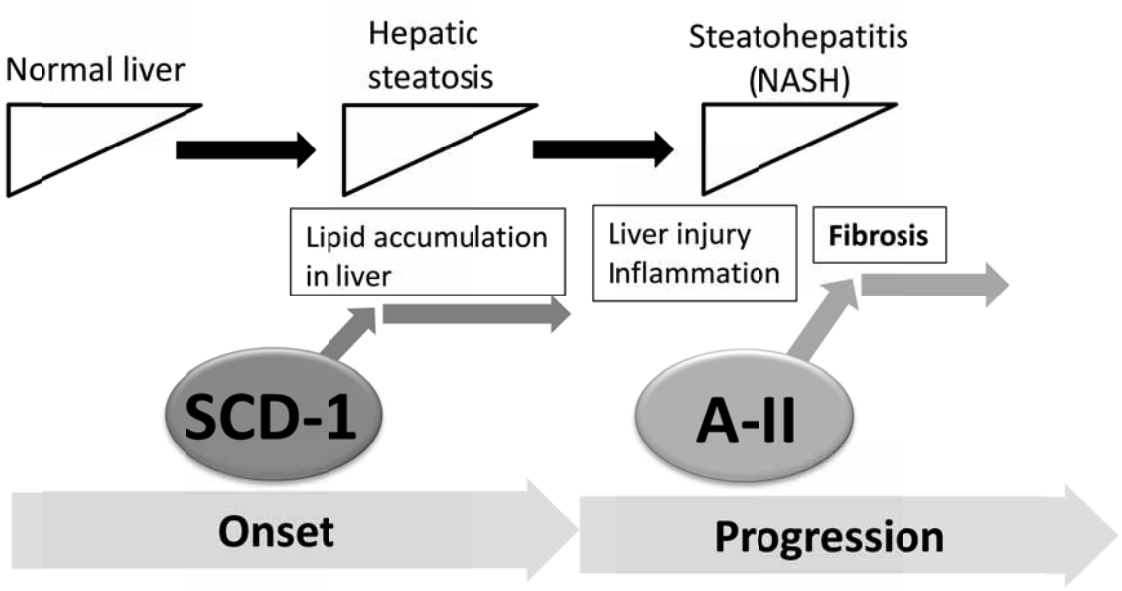

Figure 29 Summary of the effects of SCD-1 and Ang II on the onset and progression of NASH. SCD-1 contributes to develop lipid accumulation in the liver and subsequently sensitize the onset of NASH. Ang II contributes to the development of liver fibrosis.